Geobiology (2003), **1**, 91–108

Geological and trace element evidence for a marine sedimentary environment of deposition and biogenicity of 3.45 Ga stromatolitic carbonates in the Pilbara Craton, and support for a reducing Archaean ocean

MARTIN J. VAN KRANENDONK,[1] GREGORY E. WEBB[2] AND BALZ S. KAMBER[3]

[1] *Geological Survey of Western Australia, 100 Plain St., East Perth, Western Australia, 6004 Australia*
[2] *School of Natural Resource Sciences, Queensland University of Technology, GPO Box 2434, Brisbane, Queensland 4001, Australia*
[3] *Advanced Centre for Queensland University Isotope Research Excellence (ACQUIRE), University of Queensland, St. Lucia, Queensland 4072, Australia*

ABSTRACT

Bedded carbonate rocks from the 3.45 Ga Warrawoona Group, Pilbara Craton, contain structures that have been regarded either as the oldest known stromatolites or as abiotic hydrothermal deposits. We present new field and petrological observations and high-precision REE + Y data from the carbonates in order to test the origin of the deposits. Trace element geochemistry from a number of laminated stromatolitic dolomite samples of the *c.* 3.40 Ga Strelley Pool Chert conclusively shows that they precipitated from anoxic seawater, probably in a very shallow environment consistent with previous sedimentological observations. Edge-wise conglomerates in troughs between stromatolites and widespread cross-stratification provide additional evidence of stromatolite construction, at least partly, from layers of particulate sediment, rather than solely from rigid crusts. Accumulation of particulate sediment on steep stromatolite sides in a high-energy environment suggests organic binding of the surface. Relative and absolute REE + Y contents are exactly comparable with Late Archaean microbial carbonates of widely agreed biological origin. Ankerite from a unit of bedded ankerite–chert couplets from near the top of the stratigraphically older (3.49 Ga) Dresser Formation, which immediately underlies wrinkly stromatolites with small, broad, low-amplitude domes, also precipitated from anoxic seawater. The REE + Y data of carbonates from the Strelley Pool Chert and Dresser Formation contrast strongly with those from siderite layers in a jasper–siderite–Fe-chlorite banded iron-formation from the base of the Panorama Formation (3.45 Ga), which is clearly hydrothermal in origin. The geochemical results, together with sedimentological data, strongly support: (1) deposition of Dresser Formation and Strelley Pool Chert carbonates from Archaean seawater, in part as particulate carbonate sediment; (2) biogenicity of the stromatolitic carbonates; (3) a reducing Archaean atmosphere; (4) ongoing extensive terrestrial erosion prior to ~3.45 Ga.

Received 12 June 2003; accepted 05 September 2003

Corresponding author: Dr Gregory E Webb. Tel.: +617 3864 2804; fax: +617 3864 1535; e-mail: ge.webb@qut.edu.au

INTRODUCTION

Geological and geochemical evidence interpreted to support claims of very early establishment of life on Earth has come from three Early Archaean terrains: the *c.* 3.7 Ga Isua Greenstone Belt (IGB) in south-western Greenland (Rosing, 1999); the geologically unrelated 3.8 Ga rocks on the island of Akilia, 150 km south-west of the IGB (Mojzsis *et al.*, 1996); and the *c.* 3.45 Ga greenstones of the eastern Pilbara Craton in Western Australia (Dunlop *et al.*, 1978; Lowe, 1980; Walter *et al.*, 1980; Awramik *et al.*, 1983, 1988; Schopf & Walter, 1983; Schopf & Packer, 1987; Hofmann *et al.*, 1999). Claims for evidence of life preserved in the Early Archaean rocks of Greenland are based largely on the presence and isotope composition of reduced C. Whether this alone can be used to infer biogenicity has recently been questioned, with new evidence suggesting that in many samples from the IGB, reduced C is a product of metamorphic reactions (Van Zuilen *et al.*, 2002). The situation on Akilia Island is even more complex, as it is not even clear whether the analysed

carbon occurs in metasedimentary or hydrothermally altered ultramafic rocks (Fedo & Whitehouse, 2002).

It is important to stress that compared with the highly deformed, strongly metamorphosed (granulite facies) Early Archaean rocks in south-west Greenland, where the geological context is difficult, if not impossible, to reconstruct, metasediments of the Pilbara Craton are essentially undeformed and at low metamorphic grade (lower greenschist facies). Extensive mapping and petrography has firmly established the geological context in which the various supracrustal lithologies of the Pilbara Craton occur (Van Kranendonk *et al.*, 2002, and references therein). However, despite the excellent state of preservation, claims for the biogenicity of microfossils in some of these rocks have been strongly contested (Buick, 1984, 1988, 1990; Brasier *et al.*, 2002) and the biogenicity of stromatolites is equally debated (Buick *et al.*, 1981; Lowe, 1994; Lindsay *et al.*, 2003). Lindsay *et al.* (2003) have even challenged the view that the stromatolitic limestones were deposited from seawater, suggesting instead a hydrothermal origin as rigid crusts.

Overcoming problems related to testing the biogenicity of micro- and macrofossils in ancient Earth rocks is critical if we are to investigate life in the solar system. The difficulty of recognizing ancient fossils on Earth has spawned a variety of indirect geological, chemical and isotopic fingerprinting methods. However, bona fide interpretation of such fingerprints is fraught with complications (e.g. Brasier *et al.*, 2002; Schopf *et al.*, 2002), and these are greatly magnified with regard to possible evidence for biological activity on other planets (e.g. Gibson *et al.*, 2001).

In this light, we have returned to the 3.45 Ga Warrawoona Group of the Pilbara Craton in an attempt to establish some constraints on the question of biogenicity of reported stromatolites in relatively well-preserved carbonate rocks, which have never been metamorphosed to more than lower greenschist facies. The present study reports geological, petrographical and geochemical (REE + Y) data in order to test, firstly, the compatibility of a marine precipitate origin for the carbonates and, secondly, compatibility with microbial involvement in carbonate precipitation and stromatolite construction.

Rare earth element geochemistry is an appropriate means of testing the samples because the REE distribution of modern shallow seawater differs significantly from that of all known input sources, and modern and ancient carbonate rocks have been shown to record reliable marine REE signatures, with microbial carbonates providing particularly robust signatures (e.g. Holocene, Webb & Kamber, 2000; Devonian, Nothdurft *et al.*, in press; Archaean, Kamber & Webb, 2001). The concentrations of REE in seawater are controlled by different input sources (e.g. terrestrial input from continental weathering, hydrothermal input) and scavenging processes related to depth, salinity and oxygen levels (Elderfield, 1988; Piepgras & Jacobsen, 1992; Bertram & Elderfield, 1993; Greaves *et al.*, 1999). REE data can also be used to test whether the Archaean marine environment was reducing and whether terrestrial weathering was already significantly influencing marine REE chemistry by ~3.45 Ga.

GEOLOGICAL SETTING AND SAMPLE LOCATION

Sedimentary horizons that contain purported microfossils and stromatolites occur in the East Pilbara Granite–Greenstone Terrain of the Pilbara Craton, Western Australia (Fig. 1; Van Kranendonk *et al.*, 2002). Metamorphosed volcanic and sedimentary rocks (greenstones) of the Pilbara Supergroup were deposited in five autochthonous groups from 3515 to 2940 Ma, on a basement of older sialic crust as old as 3724 Ma (data in Van Kranendonk *et al.*, 2002). The thickest part of the succession is the 3490–3310 Ma Warrawoona Group (Lipple, 1975; Van Kranendonk *et al.*, 2002), which consists predominantly of basaltic volcanic rocks and subordinate ultramafic rocks erupted in a long-lived oceanic plateau (Van Kranendonk & Pirajno, in press). The Warrawoona Group also contains lesser amounts of felsic volcanic rocks and a minor amount of sedimentary rocks, the latter deposited primarily as interflow sediments and/or sediments associated with hydrothermal systems (Van Kranendonk & Pirajno, in press; Van Kranendonk in press). The sequence also contains an important carbonate unit – the Strelley Pool Chert – deposited across a regional unconformity (Buick *et al.*, 1995; Van Kranendonk, 2000; Van Kranendonk *et al.*, 2002). The Warrawoona Group is best preserved in the North Pole Dome, where it is a minimum of 18 km thick, having been deposited over ~150 Myr (Fig. 2; Van Kranendonk & Morant, 1998; Van Kranendonk, 1999, 2000; Van Kranendonk *et al.*, 2002).

Fossils have been reported from three chert horizons in the North Pole Dome (see Fig. 1 for locations). The stratigraphically lowest horizon includes both stromatolites and microfossils from bedded chert–barite–carbonate horizons in the *c.* 3490 Ma Dresser Formation (Dunlop *et al.*, 1978; Walter *et al.*, 1980; Thorpe *et al.*, 1992; Nijman *et al.*, 1998; Van Kranendonk & Morant, 1998; Van Kranendonk, 2000; Kitajima *et al.*, 2001). The cherts of this formation were previously interpreted as silicified carbonates deposited in a shallow-water, marginal marine basin (Groves *et al.*, 1981; Buick *et al.*, 1981, 1995; Buick & Dunlop, 1990), but recent studies have documented a link between deposition of the chert–barite horizons and swarms of hydrothermal chert–barite veins, active normal faulting during caldera formation and occurrence of stromatolites immediately adjacent to hydrothermal vents (Nijman *et al.*, 1998; Van Kranendonk & Hickman, 2000). Kitajima *et al.* (2001) described possible microfossils from some of the hydrothermal vein chert in the formation in a similar setting to that in the Apex chert in the adjacent Marble Bar greenstone belt, where recently debated microfossils occur (Schopf & Packer, 1987; Schopf, 1993; Brasier *et al.*, 2002; Schopf *et al.*, 2002).

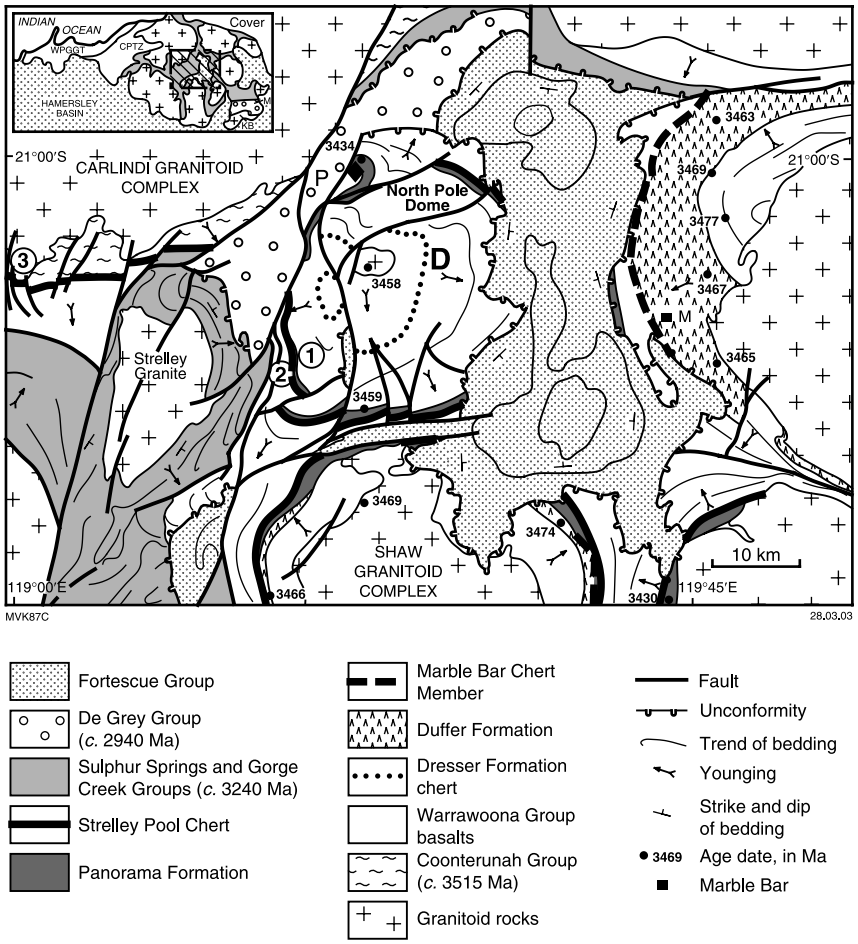

Fig. 1 Geological map of the east Pilbara, showing sample locations. Circled numbers 1–3 represent sample localities in the Strelley Pool Chert: locality 1, samples 177882 and 2-9-23; locality 2, samples 2-9-11, 2-9-14, 2-9-17, 2-9-18; locality 3, sample 2-11-15. D = Dresser Formation sample 177887 of bedded ankerite–chert 'zebra' rock. P = Panorama volcano sample 177886 of bedded jasper and siderite.

Microfossils also have been reported from ~1 km stratigraphically above the Dresser Formation in a thin (<10 m) horizon of layered white, red and brown chert that contains wrinkly laminations characteristic of stromatolites, within the Mount Ada Basalt (Awramik *et al.*, 1983). However, the age and origin of those microfossils has been the subject of contention (Buick, 1984, 1988; Awramik *et al.*, 1988) and they are not discussed further herein.

The stratigraphically highest unit is the Strelley Pool Chert, which is recognized across the 220 km diameter of the East Pilbara Granite–Greenstone Terrain and rests on older, previously deformed rocks of the Warrawoona and Coonterunah Groups across what is at least locally a high-angle unconformity (Buick *et al.*, 1995; Van Kranendonk, 2000; Van Kranendonk *et al.*, 2002, in press). The Strelley Pool Chert contains a basal clastic member and a unit of silicified and non-silicified laminated carbonates with putative stromatolites (Lowe, 1983; Hofmann *et al.*, 1999; Van Kranendonk, 2000). It has been interpreted as an evaporite unit that was deposited in a shallow-marine or sabkha-type environment (e.g. Lowe, 1980, 1983, 1994; Buick *et al.*, 1995).

We collected carbonate samples for geochemical analysis from the Dresser Formation and the Strelley Pool Chert in order to assess competing hypotheses that these units represent marine evaporite units or hydrothermal deposits. We also present results from a sample of jasper–siderite–Fe-chlorite banded iron-formation from the vent region of the 3.45 Ga Panorama volcano (Van Kranendonk, 2000) that was collected in order to compare the apparent sedimentary carbonates to a rock that contains precipitates of unequivocal hydrothermal origin (locations shown in Fig. 1).

SAMPLE DESCRIPTION

Dresser Formation

Sample 177887 is ankerite collected from a 1–2-m-thick unit of repetitively layered carbonate–chert rock (Fig. 3a,b) at the very top of the Dresser Formation, where it is conformably overlain by 10–30 cm of finely laminated, red–brown to black weathering ferruginous sediment that displays wrinkly laminations and multiple low-amplitude (1–2 cm), broad (3–12 cm) domal structures (Fig. 3c), which are identical to other such layers at various levels throughout the formation that have been interpreted as fossil microbial mats (cf. Walter *et al.*, 1980; Buick *et al.*, 1981; Nijman *et al.*, 1998). The layered

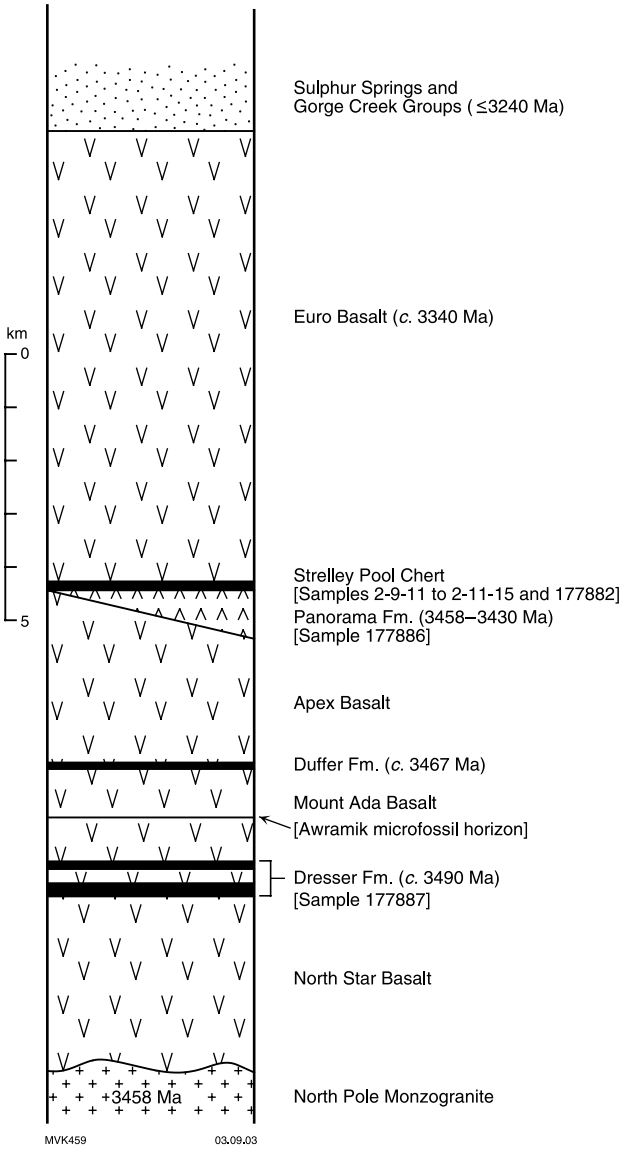

Fig. 2 Simplified stratigraphic column of the North Pole Dome, showing sample locations.

carbonate–chert rock overlies 10–20 m of layered white and grey chert with conformable barite layers and discontinuous veins of barite that lie on hydrothermally altered pillow basalt transected by numerous, subvertical chert–barite veins (Nijman *et al.*, 1998; Van Kranendonk & Pirajno, in press; Van Kranendonk, in press).

Layering in the carbonate–chert rock defines several carbonate–chert couplets (Fig. 3a,b; Van Kranendonk, in press). Carbonate layers consist of ankerite and are between 1 and 4 cm thick, whereas chert layers are generally ~1 cm thick (Fig. 3a). Contacts between lower ankerite and upper chert layers in the couplets are gradational, whereas contacts between chert layers and overlying ankerite are knife-sharp (Fig. 3b).

Strelley Pool Chert

Several carbonate samples with a variety of primary depositional textures were collected from three different localities within the Strelley Pool Chert (Fig. 1). The general stratigraphy of the formation is similar at the three localities, with a basal member of siliciclastic rocks (0.2–20 m thick) including chert boulder conglomerate and quartzite (Van Kranendonk, 2000). This is overlain by ~10–20 m of dolomitic carbonates that contain millimetre-laminations, local patches of conical and branching stromatolites, and extensive areas of crystal fans (now replaced by dolomite, but originally probably aragonite or gypsum) that interrupted bedding, as described by Hofmann *et al.* (1999) and Van Kranendonk (2000, in press). The carbonates are overlain by a siliciclastic sedimentary member that includes boulder-pebble conglomerate, sandstone and tuffaceous siltstone. The rocks of this upper member were deposited locally in several fining-upward graded units that have been interpreted as retrograding alluvial fan deposits (Van Kranendonk *et al.*, 2001).

Locality 1

This locality was originally described by Hofmann *et al.* (1999). Two samples (177882 and 2-9-23) were collected from a 7 × 3-m area of outcrop of millimetre-laminated, dark brown-weathering dolomite that contains abundant conical to branching stromatolites distributed in several onlapping biostromes (Van Kranendonk *et al.*, 2001). Lamination is mostly continuous across and between stromatolites (Fig. 4a,b). However, lamination within stromatolites is typically more even than lamination between, and on the edges of, stromatolites. In one example, pockets of flat pebbles accumulated in troughs between large (10–15 cm in amplitude), conical stromatolites (Fig. 5a,b), forming edgewise conglomerate in places (Fig. 5c). The flat pebbles are approximately 2–3 mm thick and have length to thickness aspects of >5 : 1. The pebbles do not have euhedral shapes, which are characteristic of seafloor aragonite or gypsum crystals as illustrated by Buick *et al.* (1981), and stromatolite lamination occurred preferentially on the uppermost edges of the pebbles, forming small columnar stromatolites (Fig. 5b). In some cases laminae onlap and pinch out against stromatolites (Fig. 5d). Carbonate sediments overlying the laminated horizon contain beds with tangential cross-bed sets as much as 20 cm thick (Fig. 4c).

Samples consist of millimetre-scale dolomite–quartz couplets wherein the level of silicification varies from place to place. The dolomite is equant and medium to coarsely crystalline (criteria of Folk, 1962), and the quartz forms variable equant/anhedral mosaics with crystal diameters of 50–200 μm. Sample 177882 represents a 0.25 × 0.5 × 4-cm slab cut across bedding in an area that was optically free of 'bleached' veins. The slab was cut into four pieces weighing ~100 mg (samples a–d). Sample 2-9-23 represents similar partially silicified

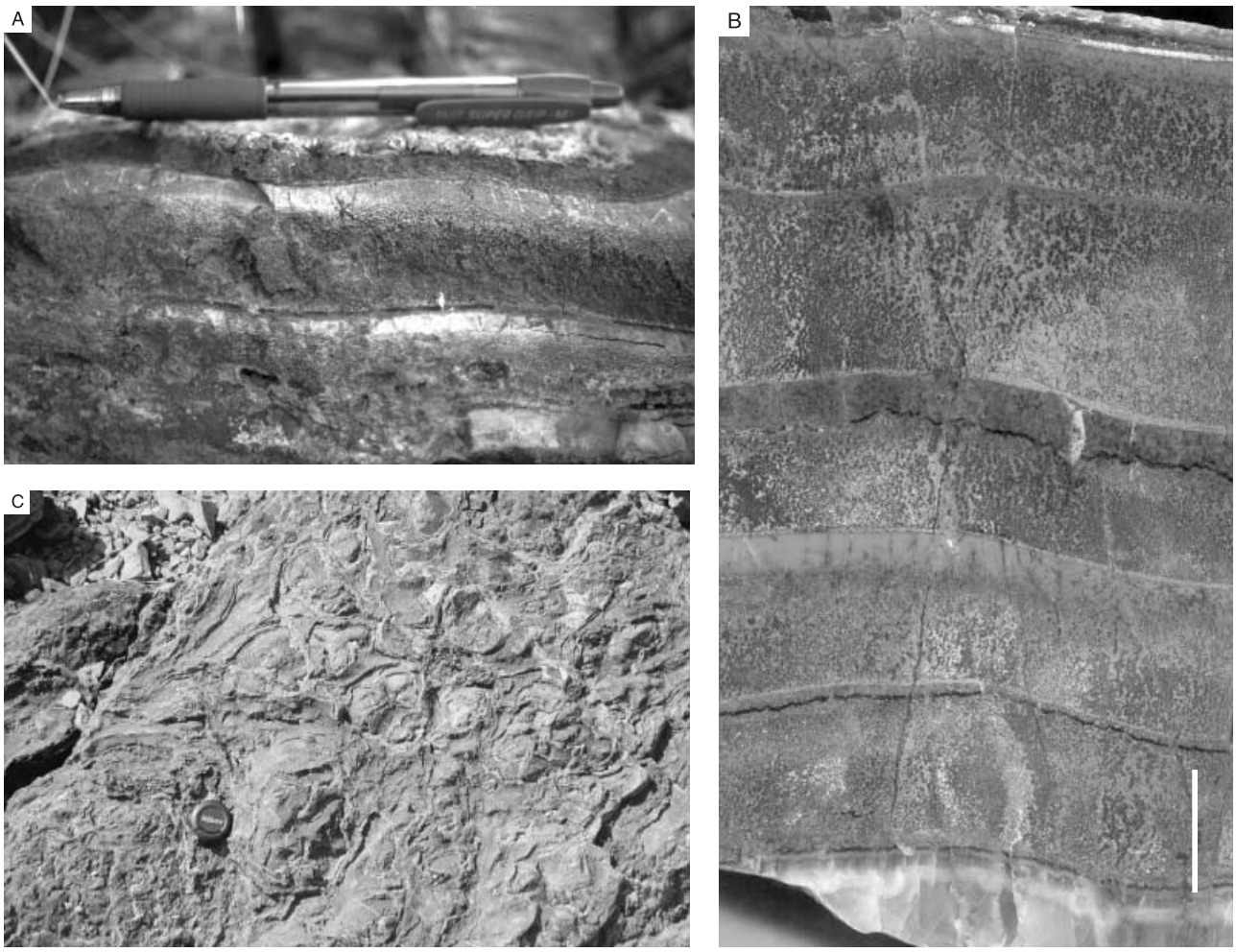

Fig. 3 Features of the Dresser Formation locality. (A) Outcrop photo of the layered carbonate–chert 'zebra' rock (sample 177887), showing repetitive layering and crystal rosettes developed in the chert layers. (B) Polished slab of the carbonate–chert 'zebra' rock, showing the gradational texture of carbonate–chert contacts and sharp nature of chert–carbonate contacts. (C) Outcrop of finely laminated material that stratigraphically overlies the layered carbonate–chert 'zebra' rock and that is interpreted as a fossil microbial mat horizon.

material collected ~2 m from a cross-cutting vertical chert vein. Samples a and b represent dolomite-rich intervals (50–100 mg) from between more silicified layers.

Locality 2

Locality 2 is ~600 m along strike from locality 1, with the same range of lithology and structures, including laminated carbonate with conical stromatolites, beds of radiating crystal fans up to 100 cm thick and wavy, laminated carbonates containing 4-cm-thick tangential cross-bed sets. Dolomite samples collected from this site include a conical stromatolite (sample 2-9-11) from which four subsamples were analysed from the crest (a and d), trough (b) and side (c) of the stromatolite. The stromatolite sample consists of equant, medium to coarsely crystalline dolomite containing less abundant, scattered, equant quartz up to 200 μm in size. Samples 2-9-17 and 2-9-18 represent less silicified layers of wavy, cross-laminated dolomite (Fig. 6a) from 1 to 2 m stratigraphically above the stromatolite sample. Both samples consist of medium to coarsely crystalline dolomite, but quartz-rich layers contain chert, and equant microquartz up to 40 μm in size. Rare quartz layers in sample 2-9-17 contain chalcedony and elongate quartz crystals radiating from the dolomite margins. The coarsest quartz mosaics contain crystals >1 mm in diametre. Euhedral dolomite crystals float in chert in some layers in sample 02-9-18. Sample 2-9-14 is from a bed of metre-long, radiating crystal fans, similar to that depicted in Fig. 6(b), from below the stromatolite layer. The sample is coarsely crystalline with scattered, rare, equant quartz crystals up to 50 μm in diameter.

Locality 3

A single sample (2-11-15) of millimetre-laminated carbonate rock (dolomite) was collected from an outcrop of the Strelley

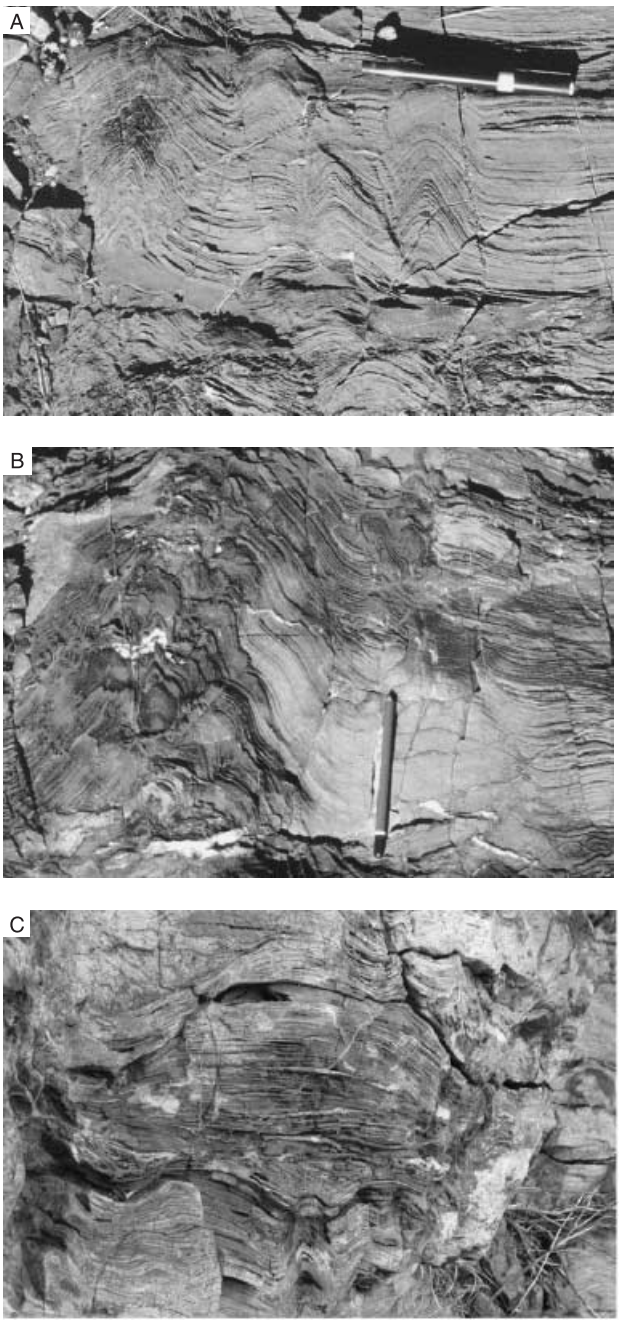

Fig. 4 Outcrop features of the Strelley Pool Chert. (A) Conical stromatolites in millimetre-laminated carbonate from locality 1. (B) Large, branching stromatolite in millimetre-laminated carbonate from locality 1. (C) Oblique view, looking down at cross-section of silicified laminated carbonate, showing large-scale cross-stratification of finely laminated carbonate sediment overlying conical stromatolite. Note cross-bedded carbonate sediments in lower left of image, on flank of stromatolite and the trough around the stromatolite.

Pool Chert ~30 km to the west of localities 1 and 2, in order to compare results over a wide area (see Fig. 1). This locality also contains conical stromatolites and crystal fans and has the same overall stratigraphy as the formation in the North Pole Dome (Barnes, 1983; Van Kranendonk, 2000). The sample consists of from base to top: (1) massive to laminated carbonate that was disrupted by isolated, radiating, hexagonal crystals, now silicified; (2) irregular laminated carbonate in which individual laminae are laterally discontinuous, consisting of convex-upward segments (subsample 2-11-15 b) (Fig. 7a); and (3) an uppermost sequence of more regular laminae that contain scattered wedge-shaped cracks that appear similar to desiccation cracks (subsample a) (Fig. 7b). The cracks are confined to individual sediment layers, but were not observed in plan-view; hence, it is unclear if they outline polygons. The dolomite throughout is medium crystalline. Quartz occurs rarely as scattered equant crystals up to 100 μm in size and in small fractures. Recrystallization has obscured the nature of crack-filling material and original lamination cannot be discerned in thin sections.

Panorama volcano

The core and volcaniclastic apron of a well-preserved felsic volcano belonging to the Panorama Formation, and dated as 3434 ± 5 Ma (Nelson, 2000), is preserved in the north-west corner of the North Pole Dome (Fig. 1; Van Kranendonk, 2000). This area consists of a shallow-dipping core zone including a basal unit of centimetre-layered jasper–siderite–Fe-chlorite banded iron-formation (BIF) up to 30 m thick, and a cross-cutting and overlying unit of coarse volcanic breccia with preserved gas vents (fumaroles) and small diatremes that fed younger eruptives (Van Kranendonk, 2000). Adjacent to the vent area is the flanking volcaniclastic apron, 2 km thick, of coarse- to fine-grained volcaniclastic rocks that were deposited during at least nine eruptive events, at least partially subaerially (Van Kranendonk, 2000). Sample 177886 is from the basal unit of BIF (Fig. 8) and includes separate subsamples of a siderite bed and a jasper bed.

METHODS

Geochemical samples (50–120 mg) were analysed for trace element concentrations using inductively coupled plasma – mass spectrometry (ICP-MS) in the ACQUIRE laboratory employing similar procedures to those outlined by Webb & Kamber (2000). Samples were cut from slabs using diamond blades and cleaned in ultra-pure water. Carbonate samples were dissolved in 15 N double distilled HNO_3; accompanying quartz is the only residual mineral and was not dissolved or analysed. Chert samples were digested in a 2 : 1 mixture of concentrated HF and HNO_3. Solutions were spiked with 10 p.p.b. of internal standards (^{6}Li, ^{84}Sr, Rh, In, Tm, Re, Bi, ^{235}U). Oxide levels were measured using pure elemental solutions, and appropriate interference correction was applied. The values for our calibration standard (W-2) are given in Table 1, as are data for international standards BHVO-1 and IFG, which were run as unknowns interleaved with the

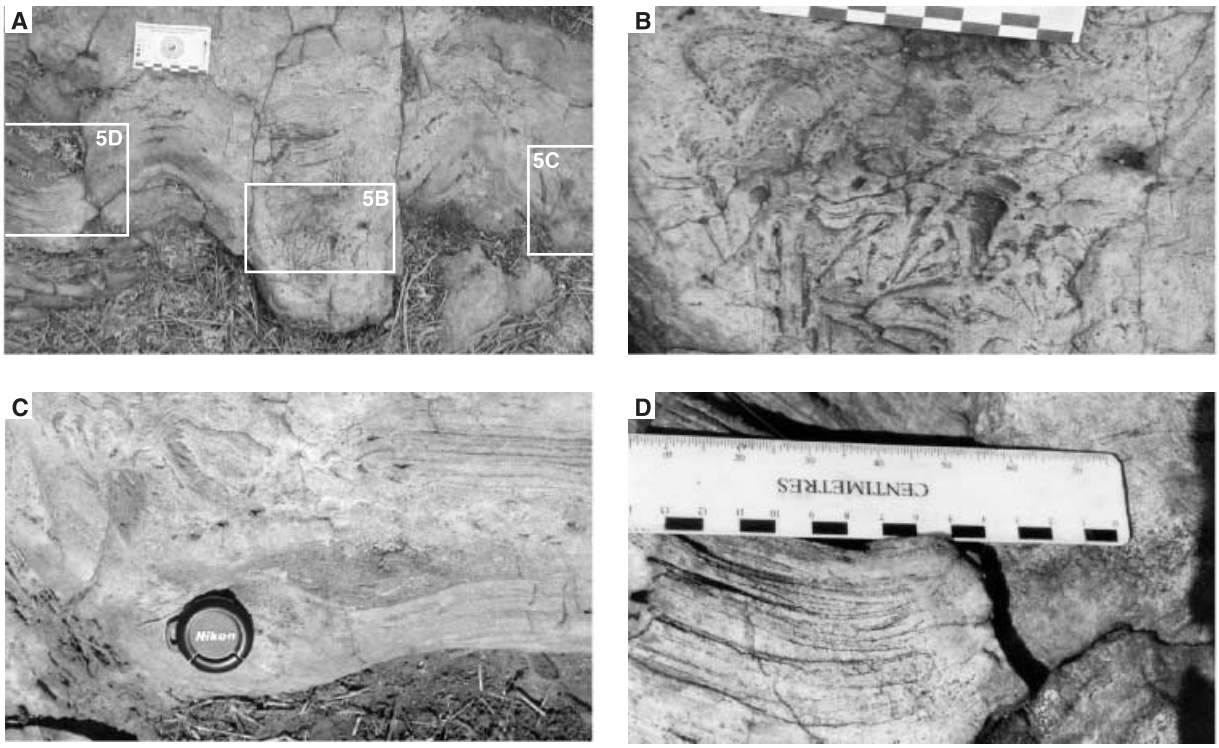

Fig. 5 Carbonate sediments from locality 1. (A) Cross-sectional outcrop view of two large, silicified, conical stromatolites, with intervening edgewise conglomerate. (B) Detail of edgewise conglomerate in (A), showing overgrowths by several small columnar stromatolites. (C) Detail of the far right-hand side of the conical stromatolites shown in (A), showing lower coarse sediment and overlying edgewise conglomerate on the flank of the stromatolite, overgrown by small columnar stromatolites. (D) Detail of the far left-hand side of (A), showing onlap of laminae on the margin of the conical stromatolite.

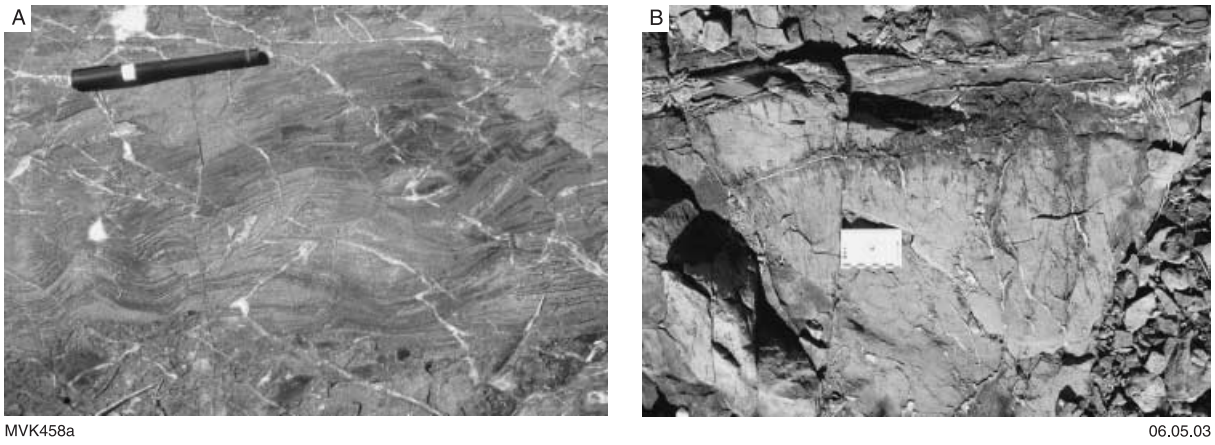

Fig. 6 (A) Wavy, rippled and cross-laminated carbonate sediments from locality 2. (B) Large crystal fans, now dolomite, from locality 1.

samples. Standard reproducibilities (1 sigma relative standard deviations) for the REE are better than 1.4% (BHVO-1) and 2.4% (IFG), and in-run errors for the REE were better than 3% in the more enriched carbonates and better than 5% in the most depleted samples. Internal errors for Sc and Th ranged from 1 to 10%, reflecting the very low concentrations. Data for the REE, Y, Sc and Th are reported in Tables 1 and 2. Data for the remaining elements will be published elsewhere.

RESULTS AND INTERPRETATION

Shale-normalized (subscript $_{SN}$, unless otherwise specified shale normalization uses PAAS, McLennan, 1989) REE + Y patterns of shallow seawater proxies have been described from both modern and ancient (Archaean) sedimentary rocks. Suitable proxies, such as microbial carbonates, BIF, certain skeletal carbonates and pristine phosphates are primarily characterized

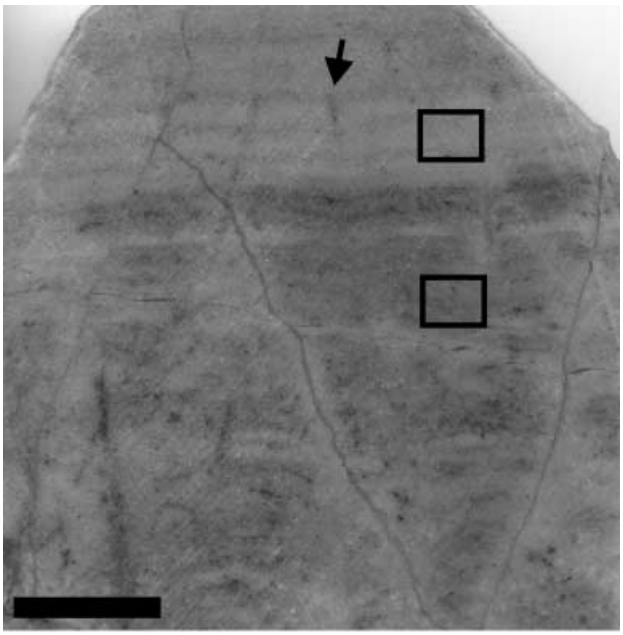

Fig. 7 Cut slab of sample 2-11-15 from the Strelley Pool Chert (locality 3), showing possible desiccation cracks (arrow) and crinkly laminae in lower half. Location of subsamples analysed for geochemistry indicated by rectangles. Scale bar = 1 cm.

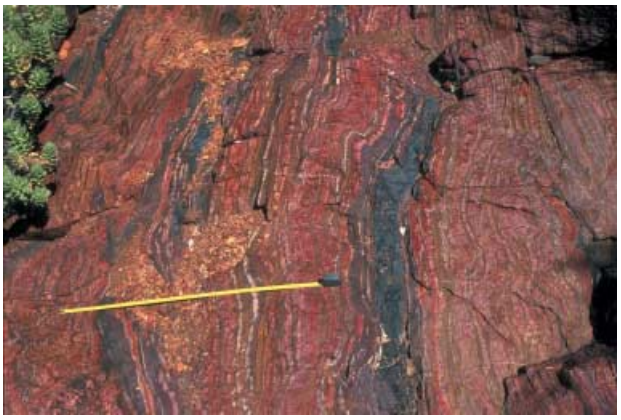

Fig. 8 Outcrop photo of jasper–siderite–Fe-chlorite from the Panorama volcano (sample 177886). Measuring tape is 1 m long.

by: (1) uniform light REE (LREE) depletion; (2) a positive La anomaly (e.g. De Baar *et al.*, 1991; Bau & Dulski, 1996); (3) distinctively high Y/Ho ratios (>44), because Y and Ho are chemically similar in charge and ionic radius, but Ho is removed from seawater twice as fast as Y owing to differences in complexation behaviour (Nozaki *et al.*, 1997); (4) minor positive Gd and Er anomalies (e.g. Alibert & McCulloch, 1993; Bau & Dulski, 1996). These features are illustrated on Fig. 9(a) by an REE + Y pattern of average Holocene microbial carbonate from Heron Reef (data from Webb & Kamber, 2000), which serves as a proxy for contemporary seawater owing to uniform seawater/carbonate partition coefficients. The concentration of Ce is additionally controlled by marine oxygenation levels whereas that of Eu also depends on (i) co-precipitation with Fe-oxyhydroxides, (ii) input from high-temperature (>250 °C) hydrothermal sources (e.g. Michard & Albarède, 1986) and (iii) more locally by Early Archaean weathering sources that are enriched in Eu relative to post-Archaean shale (e.g. Gao & Wedepohl, 1995). However, genuine REE + Y patterns can be obscured in marine precipitates by contamination with siliciclastic or volcanic detritus, both of which contain a number of robust and very different trace element fingerprints. Such contamination, as well as subsequent diagenetic and/or metamorphic overprinting, must be addressed before observed patterns can be interpreted.

North Pole Dome dolomite samples uniformly show seawater-like REE + Y_{SN} distributions characterized by light REE (LREE) depletion, superchondritic Y/Ho ratio, and positive La_{SN}, Gd_{SN} and Er_{SN} anomalies (Table 1; Figs 9b,c and 10). Siliciclastic contamination was not observed in thin sections or in insoluble residues resulting from dissolutions (only pure SiO_2), but partial silicification of some samples could have obscured such detritus. Furthermore, the relatively strong acid used for carbonate digestion could have preferentially leached REE + Y from silicates. Regardless, the presence of shale contamination (or leaching of REE + Y by acid) can be tested using Y/Ho ratios and LREE depletion. Total REE is not correlated with LREE depletion (expressed as Nd_{SN}/Yb_{SN}) (Fig. 11) or Y/Ho ratios (Fig. 12). If shale contamination were present, it would systematically decrease the level of LREE depletion and Y/Ho ratio while increasing the total REE concentration, but samples do not fall along hypothetical mixing lines produced by adding small amounts of shale contamination. Furthermore, the samples show consistent La_{SN}, Gd_{SN} and Er_{SN} anomalies, all of which suggest that the marine signature is largely intact (e.g. Bau & Dulski, 1996). Hypothetical mixing of a representative sample with PAAS shows that the anomalies become indistinct with as little as 1% shale contamination (Fig. 13). Hence, the observed patterns do not reflect contamination by siliciclastic detritus, which is also supported by low Th and Sc concentrations (Table 1).

It is unclear if the original marine precipitates were dolomite, calcite or aragonite, but they are uniformly medium to coarsely crystalline dolomite now. Hence, a certain degree of recrystallization has occurred, consistent with field observations (Barnes, 1983; Van Kranendonk, 2000). The radiating, hexagonal prism crystal fan beds were presumably originally aragonite or gypsum, but they represent secondary displacive fabrics, not original seafloor sediments, and are now mostly dolomite. In sample 02-11-15, some of the crystals have been preferentially replaced by quartz, whereas the finely laminated sediments remain dolomite, suggesting that the initial sediments were more stable than gypsum or aragonite. Hence, the sediments originally may have been calcite or early dolomite. Dolomitization of limestones and subsequent recrystallization may have varying effects on the original REE + Y pattern of

Table 1 Rare earth elements and yttrium concentrations from Warrawoona Group samples with standards

Locality Type*	2-9-11a SPC2 str.	2-9-11b SPC2 str.	2-9-11c SPC2 str.	2-9-11d SPC2 str.	2-9-23-a SPC1 str.	2-9-23-b SPC1 str.	177882-1/4 SPC1 str.	177882-2/4 SPC1 str.	177882-3/4 SPC1 str.	177882-4/4 SPC1 str.	2-9-17a SPC2 sed.	2-9-17b SPC2 sed.
Sc	250.0	337.0	309.0	340.0	223.0	445.0	232.3	204.7	229.10	174.30	784.0	1788.0
Y	1014.2	900.9	933.9	1007.2	734.6	918.8	1222.1	875.3	1386.4	802.5	7256.8	6893.7
La	56.3	52.8	52.2	50.8	46.5	60.7	119.6	80.3	142.2	76.5	567.6	498.0
Ce	85.9	79.5	78.3	81.9	53.8	70.5	135.0	75.8	157.4	77.3	704.0	666.9
Pr	14.0	12.0	13.0	13.7	7.1	8.9	14.9	8.9	18.5	9.3	97.6	96.7
Nd	77.7	68.9	76.1	77.9	29.9	39.3	64.0	37.4	78.7	38.1	514.1	517.9
Sm	45.9	37.0	43.3	47.5	13.2	14.5	16.7	12.4	21.8	13.5	251.7	244.4
Eu	27.1	21.4	24.0	27.6	8.2	8.0	10.5	6.8	13.2	7.2	119.4	123.8
Gd	89.6	78.5	89.0	103.7	30.7	29.3	38.8	24.7	45.4	23.7	557.4	564.1
Tb	13.6	11.9	13.8	16.8	4.9	5.2	6.2	4.2	7.1	4.1	103.8	101.1
Dy	70.0	62.9	73.2	91.8	34.1	40.1	51.6	31.0	56.4	32.1	655.2	629.1
Ho	17.7	15.4	17.1	20.8	9.9	10.8	15.7	10.1	17.1	10.0	156.2	153.2
Er	54.8	42.6	48.5	54.5	32.0	36.0	55.8	37.0	63.4	35.1	443.4	430.7
Yb	48.0	42.6	44.4	54.1	25.8	39.2	59.0	38.7	61.8	36.5	414.0	399.1
Lu	8.6	8.0	8.2	9.4	4.8	7.2	11.3	6.9	11.3	7.1	66.1	64.0
Th	2.0	2.3	3.5	2.6	1.6	3.6	3.3	2.5	2.9	2.6	5.7	5.7

Locality Type*	2-9-18a SPC2 sed.	2-9-18b SPC2 sed.	2-11-15a SPC3 sed.	2-11-15b SPC3 sed.	W2-9-14 SPC2 cry. fan	177887 DF ank.	177886-s PF sid.	177886-j PF jasp.	W-2 std	BHVO-1 ave.	BHVO-1 RSD	IF-G ave.	IF-G RSD
Sc	179.0	304.0	1176.0	265.0	232.0	11561.6	6992.1	15.9	36074	31874	1.67%	284.6	3.2%
Y	5144.8	7004.6	5552.3	6058.6	1139.8	6395.1	9070.2	418.7	20113	24606	0.80%	9135.3	0.5%
La	492.7	607.3	542.8	561.5	163.8	891.3	12351.4	48.4	10521	15430	0.76%	2705.6	0.5%
Ce	519.2	531.2	694.6	662.4	156.8	1441.6	20643.3	110.4	23216	38247	0.69%	3901.8	0.3%
Pr	59.7	56.6	87.7	74.4	21.5	201.0	2106.8	16.2	3025	5463	0.68%	430.2	0.4%
Nd	307.9	284.6	410.6	338.6	118.9	1059.5	7185.6	75.8	12911	24726	0.61%	1731.3	0.9%
Sm	104.8	84.2	119.6	95.7	50.5	416.2	1348.4	23.8	3266	6133	0.89%	399.0	0.6%
Eu	51.0	48.5	61.3	52.1	27.5	154.5	628.4	15.8	1094	2073	0.92%	362.1	0.4%
Gd	257.4	267.2	255.8	220.0	98.5	607.5	1330.1	37.8	3708	6291	0.79%	666.9	1.2%
Tb	40.6	39.8	40.8	34.5	14.2	111.2	216.5	7.1	615	946	0.93%	112.3	0.8%
Dy	287.3	304.4	286.6	274.9	74.6	787.6	1437.4	52.8	3808	5296	0.89%	791.4	1.7%
Ho	81.9	94.0	83.4	78.2	16.9	185.6	336.5	13.1	803	1010	0.85%	206.6	0.5%
Er	257.6	301.7	261.9	253.6	46.5	558.4	1062.7	41.5	2222	2529	0.96%	618.8	0.6%
Yb	225.3	274.5	236.9	212.0	33.5	536.3	1241.0	42.0	2058	2013	1.01%	580.2	1.4%
Lu	38.4	47.3	40.1	35.2	5.1	85.0	201.7	6.7	301	278	1.33%	90.4	2.3%
Th	7.9	1.9	9.6	8.1	2.7	20.0	1047.8	1.3	2104	1198	1.06%	43.4	3.2%

*str., stromatolite; sed., sediment; cry. fan, crystal fan; sid., siderite; jasp., jasper; ank., ankerite; ave., average.
All concentrations in parts per billion (p.p.b.).
Localites include Strelley Pool Chert locality 1–3: SPC1-3; Panorama Formation: PF; Dresser Formation: DF.
Listed values for W-2 were used for calibration.
BHVO-1 data represent an average of 254 analyses from 68 separate digestions.
IF-G data represent the average of three analyses from two separate digestions.

carbonate rocks. Banner *et al.* (1988) found that extensive early dolomitization of Carboniferous marine limestones in seawater-dominated diagenetic fluid did not alter marine REE patterns or Nd isotope values and, more importantly, that a subsequent phase of dolomitization in non-marine fluids that caused major textural recrystallization and compositional change likewise did not alter REE patterns or Nd isotope values. Jurassic dolomites from Scotland retained pristine O and C stable isotope ratios despite recrystallization during a hydrothermal/low-temperature metamorphic event (Tan & Hudson, 1971), and REE are expected to be more stable than O or C within carbonates during diagenesis because they replace Ca^{2+} in the carbonate lattice (Zhong & Mucci, 1995). However, Nothdurft *et al.* (in press) found that dolomitization of Devonian limestones associated with basement-involved, mineralizing diagenetic fluids did alter original marine REE + Y patterns, primarily affecting Ce and Y contents. Hence, the nature of the diagenetic fluid during dolomitization controls the degree of alteration of the REE + Y pattern. Additionally, subsequent dolomite/dolomite recrystallization may, or may not, alter aspects of dolomite geochemistry (e.g. Land, 1992; Machel, 1997). The well-preserved and coherent seawater-like REE + Y patterns in the North Pole Dome dolomites and their occurrence in a shallow, evaporative marine setting

Table 2 Mean rare earth element and yttrium data for different sample types from the Strelley Pool Chert

Sample type	ΣREE	Y/Ho	Nd_{SN}/Yb_{SN}	Ce/Ce*	Pr/Pr*	Eu/Eu*	Gd/Gd*	Er/Er*
Stromatolites (n = 10)	1488	70.3	0.11	0.68	0.95	2.05	1.29	1.07
2-9-23	1162	79.7	0.09	0.68	1.00	1.96	1.24	1.10
177882	1581	80.9	0.09	0.67	0.97	2.06	1.26	1.14
2-9-11	1558	54.3	0.13	0.71	0.92	2.07	1.31	1.00
Sediments (n = 6)	9788	62.1	0.11	0.68	0.91	1.61	1.24	1.06
2-9-17	11645	45.7	0.11	0.69	0.92	1.53	1.16	1.01
2-9-18	8907	69.1	0.10	0.63	0.86	1.61	1.39	1.11
2-11-15	8813	71.8	0.14	0.72	0.94	1.81	1.31	1.12
Bladed crystal (n = 1)								
2-9-14	1968	67.5	0.30	0.59	0.89	2.10	1.38	1.06

ΣREE expressed in parts per billion (p.p.b.). Y/Ho based on raw elemental abundance. All other columns represent shale-normalized data.

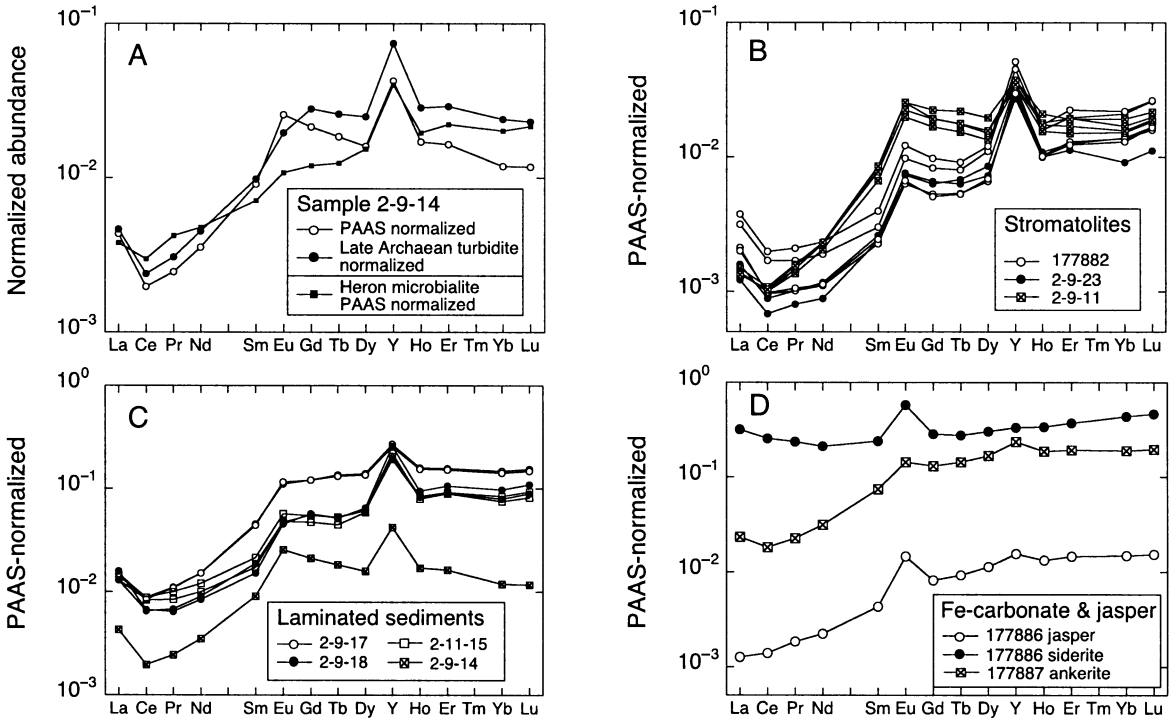

Fig. 9 Shale-normalized (using Post-Archaean-Australian-Shale, PAAS of McLennan, 1989) REE + Y patterns of Warrawoona Group samples. (A) Comparison of patterns for sample 02-9-14 normalized using PAAS and an average of HREE-depleted turbidite (solid squares) from the Late Archaean Yellowknife greenstone belt (average of most HREE-depleted samples Y-10 A1, Y-18 A, Y-19 A, Y-22 A, Y-27 A, Y-27 E; Yamashita & Creaser, 1999). PAAS-normalized Holocene microbialite is shown for comparison (data from Webb & Kamber, 2000). (B) REE + Y_{SN} patterns for Strelley Pool Chert stromatolite samples from localities 1 and 2. Note the smooth patterns, LREE depletion, and positive La and Y anomalies, which are characteristic of shallow seawater. Additionally, note the absence of a negative Ce anomaly and the prominent positive Eu anomaly, which suggest that the shallow seawater was reducing. (C) REE + Y_{SN} patterns for Strelley Pool Chert particulate sediments and radiating crystal fan sample (02-9-14; X in square) from localities 2 and 3. Note that sediment patterns have smooth LREE depletion, positive La, Y and Er anomalies, which are characteristic of shallow seawater, plus a pronounced positive Eu anomaly and the lack of a negative Ce anomaly. The radiating crystal fan REE + Y pattern appears to have lost HREE preferentially. (D) REE + Y_{SN} patterns for Dresser Formation ankerite and Panorama Formation siderite and jasper. Note the smooth seawater-like pattern of the Dresser Formation ankerite (X in squares). It is similar overall to sediment samples from the Strelley Pool Chert except for the relatively low, but still superchondritic, Y anomaly. The Panorama Formation siderite pattern (filled circle) is very smooth, showing no Y anomaly and insignificant LREE depletion, but it has a very large positive Eu anomaly. The pattern is unlike shallow seawater and is interpreted as representing precipitation from a hydrothermal fluid. The Panorama jasper (open circle) REE + Y pattern is more seawater-like, having pronounced LREE depletion, but it lacks the characteristic La anomaly and has a very small Y anomaly. It is interpreted as representing hydrothermal fluid intermixed with, or containing remnant elements of, seawater.

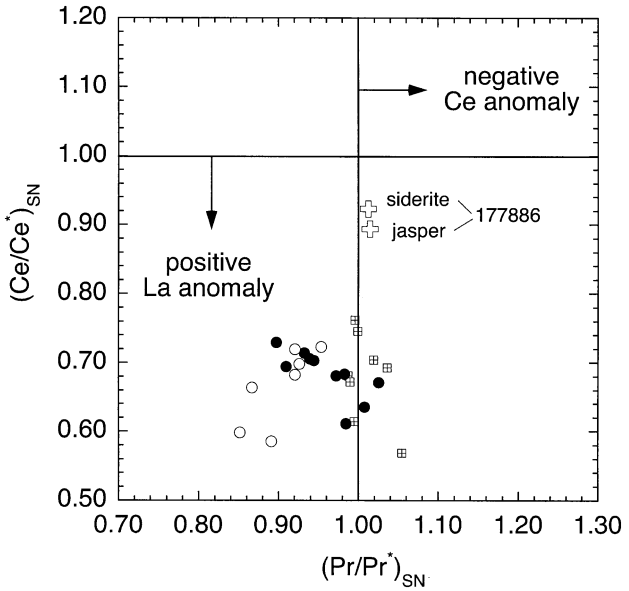

Fig. 10 Diagram discriminating between La and Ce anomalies. In samples with no negative Ce anomaly, a positive La anomaly exists when Ce/Ce* ($[Ce/(0.5La + 0.5Pr)]_{SN}$) is smaller than unity. A negative Ce anomaly exists in samples where Pr/Pr* ($[Pr/(0.5Ce + 0.5Nd)]_{SN}$) is greater than unity. The studied stromatolite samples (solid circles) plot into an area characterized by a significant positive La anomaly but no significant Ce anomaly. An almost identical field is occupied by late Archaean stromatolites (crossed squares) from the Campbellrand platform (data from Kamber & Webb, 2001). There also is excellent overlap in the extent of La anomaly with the laminated carbonate sediments studied here (open circles), which in terms of Ce suggest a small positive anomaly not previously described from such rocks. The hydrothermal siderite from sample 177886 and the interlayered jasper plot in an entirely different position, lacking both La and Ce anomalies.

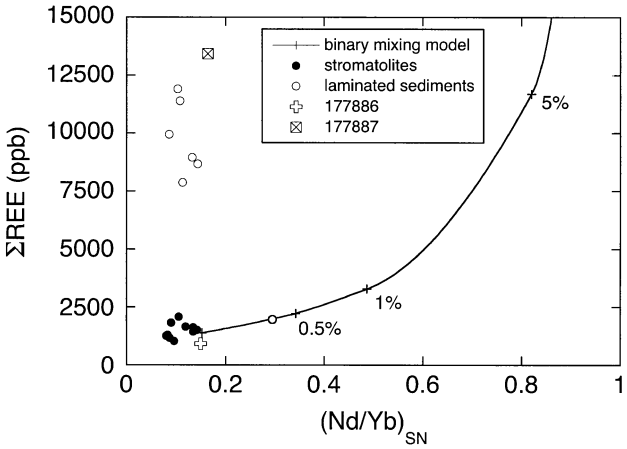

Fig. 11 Shale-normalized Nd/Yb ratio vs. total REE content (in p.p.b.) of studied stromatolites, laminated carbonate sediments, 177886 jasper and 177887 ankerite. Note that the hydrothermal 177886 siderite sample plots off scale at much higher total REE content (59 160 p.p.b.). The important observation is that there is no correlation between extent of LREE depletion (low Nd/Yb) and total REE content as would be expected from shale contamination (shown is a hypothetical mixing line resulting from PAAS admixture). The majority of laminated carbonates have higher total REE than samples preserving sedimentological features of stromatolites but this must be due to more efficient REE uptake from seawater rather than shale contamination. Only sample W2-9-14 plots along the PAAS mixing hyperbola, but more likely as a result of subsequent HREE loss than to shale contamination.

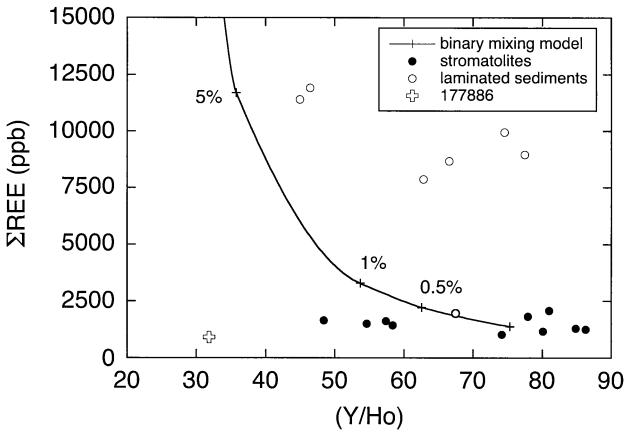

Fig. 12 Y/Ho ratio vs. total REE content (in p.p.b.) of stromatolites, laminated carbonate sediments and 177886 jasper. Note that the hydrothermal 177886 siderite sample plots off scale at much higher total REE content. There is no correlation between Y/Ho and total REE content in the stromatolites, implying that the Y/Ho ratio of waters from which they precipitated was as variable as in modern seawater. Only three of the laminated sediments plot close to the binary mixing line, whereas the other samples have high REE totals but still high Y/Ho, contraindicating contamination with shale as the reason for high REE content.

(e.g. Lowe, 1983, 1994; Buick & Dunlop, 1990) is consistent with early dolomitization in seawater-dominated fluids. The consistent REE + Y patterns of Strelley Pool Chert samples over an areal extent of ~30 km suggest that subsequent diagenetic recrystallization did not significantly alter the patterns.

Strelley Pool Chert samples

Stromatolite samples are characterized by seawater-like REE + Y_{SN} patterns (Table 2; Fig. 9b). Samples 177882 and 2-9-23 from locality 1 show very similar patterns with very large LREE depletion (mean $Nd_{SN}/Yb_{SN} < 0.1$) whereas sample 2-9-11 from locality 2 shows a flatter mid- to heavy REE (HREE) pattern (mean $Nd_{SN}/Yb_{SN} = 0.13$), a smaller Y/Ho ratio, and a less uniform, smaller La anomaly. All stromatolite samples have a substantial positive Eu_{SN} anomaly (~2) and lack a Ce_{SN} anomaly (Fig. 10). Readers not familiar with distinction between positive La anomaly and negative Ce anomaly are referred to Bau & Dulski (1996), Webb & Kamber (2000) and Kamber & Webb (2001) for more detailed explanations. Sediment samples from locality 2 (Fig. 9c) have intermediate LREE depletion (mean Nd_{SN}/Yb_{SN} ~ 0.1), Y/Ho ratios similar to 2-9-11 (45, 69) and positive La anomalies, but have higher total REE concentrations than all stromatolites (8907–11 645 p.p.b. compared with 1161–1581 p.p.b). The distant locality 3 Strelley Pool

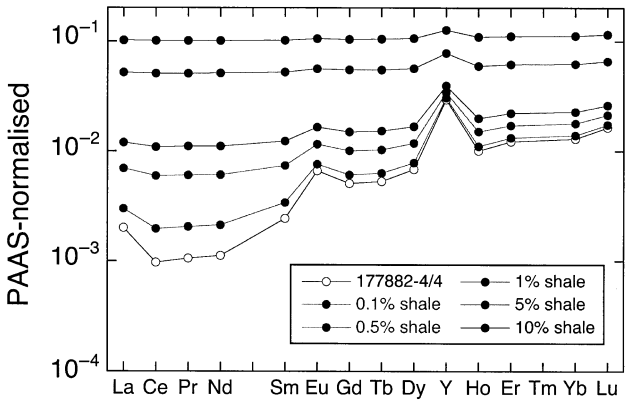

Fig. 13 Calculated REE + Y patterns of shale-normalized samples containing a mixture of stromatolite sample (177882–4/4) and PAAS. Even small amounts of shale contamination (e.g. 1%) alter the REE + Y pattern significantly while greatly increasing the total REE content.

sample (2-11-15) has a similar REE + Y pattern to the locality 1 stromatolites (mean $Nd_{SN}/Yb_{SN} = 0.13$, $Y/Ho = 72$), but also has a high total REE (8813 p.p.b.).

The final Strelley Pool sample 02-9-14 represents a dolomitized replacement of radiating crystal fans. The crystals disrupted lamination in the sediment and are interpreted as secondary crystal growth below the sediment–water interface. The crystal fan sample differs from all other Strelley Pool samples in having the least (although still well within the range of modern seawater) LREE depletion ($Nd_{SN}/Yb_{SN} = 0.30$) and slight HREE depletion (i.e. $Tb/Lu > 1$) (Fig. 9c). The sample retains positive La_{SN}, Eu_{SN}, Gd_{SN} and Er_{SN} anomalies and has a seawater-like Y/Ho ratio (= 67.5), but appears to be depleted in HREE. This could be an artefact of normalization (with PAAS) or reflect genuine HREE loss. The former possibility is illustrated on Fig. 9(a), where the REE + Y pattern for sample 02-9-14 is normalized with a late Archaean turbidite average. This shows that if the local seawater was more HREE depleted (possibly due to a preponderance of tonalite weathering), sample 02-9-14 no longer shows HREE depletion, but a generally flat pattern across the HREE. This alternative normalization also illustrates the variability in Eu anomaly of local input sources. Alternatively, the sample may have been affected by secondary loss of HREEs to seawater. Secondary release of HREEs from sediments occurs in modern estuaries where there is extensive resuspension of sediments in very shallow, mid-salinity waters (Sholkovitz & Szymczak, 2000). A similar process may have affected the other samples from locality 2 to a lesser extent, with the sediment patterns being modified somewhat less than the stromatolites owing to their larger initial REE concentrations or higher stratigraphic position. Irrespective of the true reason for the variation in HREE slope, we note that the feature appears to be related to depositional setting. The overall sequence is interpreted as having deepened-up on the basis of the exposure-related jasper-bearing conglomerate at the base and overlying pillow basalts. Hence, the decreasing HREE depletion from the crystal fan, through stromatolite to sediment samples could reflect a deepening environment where sediments interacted less with the shallow estuarine waters up section, or where the shallowest samples precipitated from water with a more local (tonalite-like) REE composition.

Dresser Formation

The ankerite sample (177887) from the Dresser Formation also has a seawater-like REE + Y pattern (Fig. 9d), with large LREE depletion ($Nd_{SN}/Yb_{SN} = 0.16$) and positive, but small La_{SN}, Gd_{SN} and Er_{SN} anomalies, but differs from the Strelley Pool Chert carbonates in having a low Y/Ho ratio (= 34.5), which is still significantly higher than the chondrite average (note that relative to our preferred calibration standard, we obtain a chondritic Y/Ho of 25.4 ± 0.6). The total REE concentration is the highest of all samples except for the Panorama hydrothermal siderite sample.

Panorama Formation

The siderite sample from BIF from the Panorama Formation has the highest total REE concentration of all samples (59 160 p.p.b.) and shows a distinctly non-seawater-like REE + Y pattern (Figs 9d and 14) including: (1) a smooth pattern with LREE enrichment from Nd_{SN} to La_{SN}, but HREE enrichment from Nd_{SN} to Lu_{SN}; (2) no positive La_{SN}, Gd_{SN} or Er_{SN} anomalies; and (3) a near-chondritic Y/Ho ratio of 27. Although the REE + Y distribution coefficients between fluids and Fe-carbonates remain to be determined, we note that the Dresser Formation ankerite (above) resembles the patterns recorded in dolomite. When comparing the siderite REE + Y pattern with patterns of modern hydrothermal vent fluids from mid-ocean ridges, the possibility of a systematic rotation of the pattern's slope has to be considered because partition behaviour could vary with atomic number. Nonetheless, there are two significant observations that allow interpretation despite these limitations. First, the siderite REE + Y pattern is very smooth. As discussed above, seawater samples, and proxies thereof, show very significant abundance spikes (and deficiencies) in a number of REE and Y, a feature that originates from differences in stabilities of REE + Y surface complexes in hydrous solutions (e.g. Bau, 1999). By contrast, REE patterns of hydrothermal vent fluids sampled at mid-ocean ridges are smooth (except for the redox-sensitive Ce and Eu). This is best appreciated in datasets obtained by ICP-MS (e.g. Bau & Dulski, 1999; Douville *et al.*, 1999, 2002). There is considerable variation in slope (Fig. 14a) of shale-normalized patterns of modern vent fluids (e.g. Michard & Albarède, 1986; Douville *et al.*, 1999), reflecting secondary phase precipitation and phase separation superimposed on the general pattern that is controlled by fluid–rock interaction. The uniting feature of all oceanic hydrothermal vent fluids is

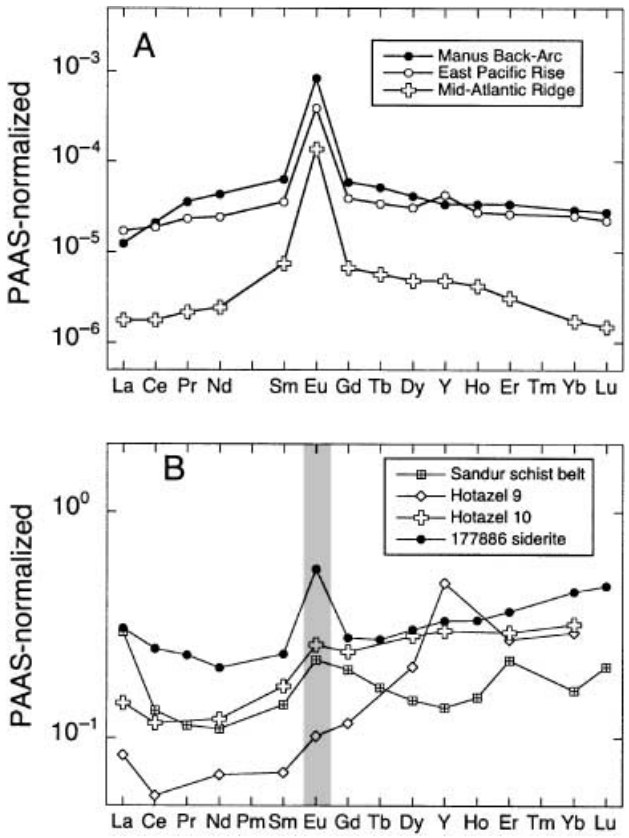

Fig. 14 (A) PAAS-normalized REE + Y patterns of vent fluids from mid-ocean ridges (Atlantic sample is Division 1.3 G1; East Pacific sample is ND 17 G2) and a back-arc basin (Manus) (all data from Douville *et al.*, 1999). (B) Comparison of 177886 siderite REE + Y pattern with other Precambrian siderite (dominated) REE + Y patterns. The pattern of the Late Archaean Sandur schist belt was plotted from the average ($n = 28$) of Fe–Mn carbonate formation reported by Manikyamba & Naqvi (1995). The Early Proterozoic patterns of the Hotazel banded iron-formation were plotted from siderite-dominated samples 9 and 10 reported by Tsikos & Moore (1997).

the presence of a positive Eu anomaly, which reflects strong REE complexation by chloride ions and REE + Y partitioning between oceanic rocks and the fluid as the latter migrates to the surface. To our knowledge, the studied siderite from the Panorama Formation BIF, which displays a strong positive Eu anomaly in an otherwise smooth pattern (Figs 9d and 14a,b), is the first verification of the long-held conjecture that Archaean hydrothermal input into the ocean was evident from the positive Eu anomaly in seawater proxies (Derry & Jacobsen, 1990).

The accompanying jasper sample, which is also regarded as a hydrothermal precipitate, has a much lower total REE concentration (910 p.p.b.) and a somewhat more seawater-like REE + Y pattern with high LREE depletion ($Nd_{SN}/Yb_{SN} = 0.15$), but no real La_{SN}, Gd_{SN} or Er_{SN} anomalies and a Y/Ho ratio of only 31.8 (Fig. 9d). Certain modern low-temperature hydrothermal springs, particularly from ridge flanks, also carry residual seawater features (e.g. elevated Y/Ho, small positive La anomaly; Wheat *et al.*, 2002), and these features are generally interpreted to indicate different styles of water–rock interaction at lower temperatures and/or a much reduced rock-to-fluid ratio. Such fluids are much poorer in other dissolved species (e.g. REE), but are higher in Mn, Co, Ni, Zn, Cd and Mo than bottom seawaters. Therefore, our preferred interpretation of the cyclical siderite–jasper bands is precipitation along an oceanic volcanic system in which periods of input of high-temperature fluids (siderite) alternated with periods of reduced hydrothermal activity, during which the fluids retained some seawater characteristics (jasper). A model of the setting in which these rocks formed is a volcanic caldera with an outlet to the ocean, similar to that documented for Satonda Crater, an active volcano in Indonesia (Kempe & Kazmierczak, 1990). During periods of intense hydrothermal activity, the caldera was saturated with hydrothermal fluids and siderite was precipitated, whereas in intervening periods normal seawater filtered back, hydrothermal activity was reduced and water–rock exchange occurred at lower temperature. The caldera scenario also offers an attractive explanation for the presence of jasper in an anoxic global marine environment. Namely, the limited volume of water in a (temporally) confined caldera could undergo a change in redox conditions much more readily than a body of water in open contact with the buffering ocean. Whether photosynthesizing microbes existed, fluctuating biological productivity in the caldera could be the force driving the redox changes reflected in the alternating jasper–siderite laminae. We note that in the Satonda caldera, rim-dwelling microbes play an important role in chemical stratification of the caldera water (e.g. Konhauser *et al.*, 2002). Hence, the restriction to open ocean water exchange afforded by a volcanic caldera could have permitted the creation of 'islands of productivity' in an otherwise hostile global marine environment.

DISCUSSION

Archaean seawater

The similarity of Strelley Pool Chert carbonate REE + Y patterns to those of modern seawater suggests that the primary processes that control REE distribution in modern seawater were already operating by ~3.45 Ga. The only differences are: (1) higher LREE depletion, (2) a strong positive Eu anomaly and (3) the lack of a strongly negative Ce anomaly in all studied Archaean samples. As the REE distribution of modern shallow seawater is controlled primarily by the balance between input from marine hydrothermal and terrestrial weathering inputs as modified by scavenging in estuarine and deeper marine environments (Elderfield, 1988), similar processes appear to have been in place in the Archaean.

Very high LREE depletion compared with modern seawater probably has several causes. Preponderance of basaltic REE

sources in general (Condie, 1993) could have contributed to this feature, but removal processes have greater potential to affect the slope of marine REE patterns. Bau & Möller (1993) and Alibert & McCulloch (1993) have suggested that HREE enrichment relative to LREE could reflect higher CO_2 pressure and hence different marine pH, favouring HREE stability in the water column. More efficient removal of LREE in estuaries presently occurs with organic/clay complexation or carbonate complexation in estuaries where salinity increases from 2 to 10‰ (Hoyle *et al.*, 1984). By analogy, our data could imply that by 3.45 Ga, sufficient freshwater entered the ocean to induce significant LREE scavenging on a large scale. Whether the deeper LREE depletion of the ancient samples could be related to fresh water meeting hypersaline waters of an evaporative environment remains to be established, but the presence of oxyhydroxides, such as those that occur in modern river water, is contraindicated. Because the extent of negative Ce anomalies in modern shallow waters is variable and sometimes insignificant, its absence in a single Precambrian carbonate cannot be used to argue for anoxic conditions. However, we note the persistent and systematic lack of negative Ce anomalies not only in this new dataset but from all other high-quality complete REE + Y datasets of Archaean hydrogenous sediments, which we interpret as a strong indication of insufficient free O to oxidize Ce to (IV) state. Under sufficiently oxidizing conditions, Ce is removed very early with Fe oxides in the river water (e.g. Sholkovitz, 1992). Importantly, where such oxyhydroxide complexes were preserved in Devonian estuarine carbonate sediments, they have a positive Ce anomaly (Nothdurft *et al.*, in press).

For reasons explained in detail previously (Kamber & Webb, 2001), the high Eu concentrations also preclude the presence of oxygenated waters in the deep marine environment. In brief, under oxidizing conditions, REE + Y from hydrothermal vent waters are co-precipitated with seafloor Fe oxyhydroxides. As a result, hydrothermal vents are presently sinks for oceanic REE + Y (Bau & Dulski, 1999). The presence of a positive Eu anomaly in relatively shallow marine 3.45 Ga precipitates thus not only indicates a greater hydrothermal flux, but also that the REE + Y from hydrothermal vents were not immediately co-precipitated. The interrelationship between hydrothermal Fe and REE + Y input explains the divergence of oceanic Nd- and Sr-isotope evolutions in the ocean after the oxidation of the deep ocean waters (Kamber & Webb, 2001).

Biogenicity of Strelley Pool Chert Stromatolites

Hofmann *et al.* (1999) discussed the locality 1 Strelley Pool Chert stromatolites in some detail and firmly rejected the possibility that the stromatolites could represent post-depositional deformation structures. Those arguments need not be repeated here, although additional data discussed below support their case and further indicate that the structures had syndepositional relief on the seafloor. Lowe (1994) suggested that the conical stromatolites lack many of the important criteria for biogenicity as defined by Buick *et al.* (1981). Although Lowe (1994) could not discount a biological origin, he interpreted the structures as accumulations of rigid seafloor crusts that had hard surfaces during deposition. Such rigid crusts could have resulted from biologically induced precipitation, but are widely considered to be abiotic in origin (e.g. Grotzinger, 1994; Grotzinger & Knoll, 1995; Grotzinger & Rothman, 1996; Pope *et al.*, 2000). Regardless, Lowe (1995) noted that there are still no known definitive inorganic analogues for such conical accumulations of rigid crusts, although somewhat similar conical stromatolites in the Palaeoproterozoic Pelthei Group of Canada were interpreted as more or less abiotic seafloor precipitates (Pope *et al.*, 2000). Strelley Pool Chert stromatolites differ significantly from the Pelthei precipitates described by Pope *et al.* (2000) in that the laminae are commonly not isopachous from the stromatolites to surrounding areas, typically being finer on the stromatolites and coarser and less regular in off-stromatolite areas (Figs 4 and 5). Additionally, many Strelley Pool Chert stromatolites do not diverge upwards as in Pelthei Group precipitates that were considered to represent abiotic rigid crusts (Pope *et al.*, 2000; Fig. 4).

Lindsay *et al.* (2003) also interpreted the Strelley Pool Chert stromatolites as rigid crusts and additionally suggested that they were abiotically deposited from hydrothermal fluids. However, our Strelley Pool Chert REE + Y data firmly refute a hydrothermal origin for the stromatolites. As the stromatolites and particulate sediments both retain seawater-like REE + Y patterns, there is little likelihood that they represent anything other than normal shallow-marine carbonates. Archaean seawater was clearly more affected by hydrothermal fluids than modern seawater, but the contrast between the REE + Y profiles of the stromatolites relative to that of hydrothermal siderite from the Panorama Formation (e.g. Fig. 9b,d) and to the signature of modern hydrothermal fluids (Fig. 14a) clearly indicates that the stromatolites were not precipitated directly from hydrothermal fluids.

Lowe's (1994) specific arguments against biogenicity for Strelley Pool Chert stromatolites include the following: (1) the structures lack wavy or crinkly laminae, (2) sediment was unlikely to have been trapped and bound on the steep sides of the structures, (3) the lack of detritus between stromatolites suggests that little 'loose detritus' was available for trapping and binding, and (4) there are no reworked pieces of 'mat material' in surrounding sediment. New evidence from recent fieldwork allows many of Lowe's (1994) specific criticisms to be re-examined and his interpretation of the stromatolites as rigid crusts to be rejected.

(1) Despite Buick *et al.*'s (1981) contention that biogenic stromatolites must have wavy or crinkly laminae, many biogenic stromatolites from a variety of settings and times had relatively

smooth continuous lamination at the scales observable in the Strelley Pool Chert samples. The degree of recrystallization and secondary silicification in Strelley Pool Chert samples would have obscured any original fine-scale crinkly or irregular lamination, and lamination at larger scales is not completely uniform and regular at locality 1 in any case. Hence, the apparent lack of wavy and crinkly lamination may be an artefact of preservation. Dolomitization and/or recrystallization also obscured sediment grain boundaries in the cross-bedded samples from locality 2 (02-9-17, 02-9-18), but the overall cross-lamination remains visible. The sample with the finest crystalline fabric, sample 02-11-15 from locality 3, is very similar in appearance to crinkly algal mat fabric, and its interpretation as such would be trivial if not for the age of the sample. In that case the laminae are flat-lying and do not form relief-bearing stromatolites, but more irregular lamination is preserved where recrystallization was less coarse, and that sample shares a very similar REE + Y pattern with the locality 1 stromatolites.

(2) Lowe's (1994) suggestion that the steep sides of the Strelley Pool stromatolites could not be produced by trapping and binding of sediment is untenable. The induction of precipitation within microbial biofilms has been emphasized increasingly, relative to trapping and binding, as an important part of microbialite formation (e.g. Reitner, 1993; Webb *et al.*, 1998; Riding, 2000), and many microbialites, laminated and non-laminated, have been demonstrated with steep to overhanging relief. There is little question as to the biogenicity of Proterozoic *Conophyton*-like stromatolites that have similarly steep and steeper, laminated sides.

(3) Lowe's (1994) suggestion that there was no 'loose detritus' to be trapped and bound has also been refuted by recent fieldwork. Cross-laminated samples clearly represent loose sand-sized sediment because the cross-lamination sets are too thick (6–20 cm) to represent bedforms made in silt or mud. Hence sand-sized carbonate sediment must have existed in the environment. The cracked laminae in sample 02-11-15 (locality 3) also suggest the deposition of particulate sediment, and further, that deposition was cyclical, thus forming lamination. In that case, the grain size was much finer, as wedge-shaped cracks would not be expected to form in coarser sand-sized laminae. Irrespective of whether the cracks represent desiccation cracks on the surface, or if the cracking occurred subsequently owing to dewatering during shallow burial, the differential volume change from the bottom to top of the lamina that resulted in the wedge-shaped cracks suggests that the material was not lithified and clearly did not represent a rigid seafloor crust. Laminae that onlap, and pinch out against, stromatolites also suggest deposition of particulate sediment in the immediate vicinity of the stromatolites (e.g. Fig. 5). Such structures are incompatible with formation of laminae as rigid crusts. Although recrystallization does not allow individual sediment grains to be observed in the stromatolites or intervening areas, the stromatolites have the same bulk chemical composition as the cross-bedded and cracked sediments on the basis of the similar REE + Y patterns (e.g. Fig. 9b,c). Additionally, there is no suggestion of palisade structure or other orientated larger crystal fans or aggregates within the laminae as commonly occur in seafloor cement crusts (e.g. Grotzinger & Knoll, 1995).

(4) Lowe's (1994) contention that there was no evidence of reworked pieces of 'mat material' in sediments associated with the stromatolites also can be rejected. Accumulations of flat pebbles that form edgewise conglomerate between stromatolites at locality 1 (Fig. 5) almost certainly resulted from erosion of the stromatolite-forming laminae. Such edgewise conglomerates are particularly common in peritidal algal mat–stromatolite associations in Proterozoic and early Palaeozoic carbonate deposits (e.g. Bertand-Sarfati & Moussine-Pouchkine, 1998). Erosion of very thin flat pebbles indicates that stromatolite lamination cannot consist entirely of rigid seafloor crusts. Such crusts would not be expected to erode into individual laminae. Rather, they suggest that the laminae contained unconsolidated particulate sediment with some layers undergoing partial lithification very early on the sea floor. Better-indurated layers were ripped up during storm events and deposited in lows between stromatolites. The edge-wise configuration probably resulted from wave agitation. Alternatively, the pebbles could consist of layers of rigid seafloor crust that were isolated between less well-indurated particulate sediment, but regardless, less well-indurated, particulate sediment must have accumulated on the steep-sided structures.

Hence Lowe's (1994) interpretation of the Strelley Pool Chert stromatolites as accumulations of rigid seafloor crusts can be refuted, and the presence of flat pebble conglomerates actually requires that the structures contained layers of poorly indurated sediment. The similarity of REE + Y patterns in the stromatolites and demonstrably particulate sediment samples reinforces this interpretation. That, combined with the steep sides of the structures (40–75°), suggests that some type of trapping and binding was required, even if some laminae represent crusts precipitated directly from seawater (cf. Hofmann *et al.*, 1999). Hence, the trapping and binding of particulate carbonate sediment and robust seawater-like REE + Y pattern exhibited by the stromatolites are completely consistent with microbially induced precipitation, which elsewhere has recorded robust signatures of ambient seawater REE + Y geochemistry (e.g. Webb & Kamber, 2000; Kamber & Webb, 2001; Nothdurft *et al.*, in press).

CONCLUSIONS

The results of detailed mapping, petrography and REE + Y geochemistry of Early Archaean carbonate rocks from distinct formations in the Warrawoona Group, east Pilbara has shown the following:

1 Laminated dolomites in the ~3.45 Ga Strelley Pool Chert were deposited as primary carbonate sediments and retain

well-preserved, robust and reproducible REE + Y signatures indicating deposition from shallow seawater.

2 The REE + Y geochemical evidence combined with new sedimentological observations, including edgewise conglomerates, suggest that laminated conical stromatolites in the Strelley Pool Chert are composed at least partly of particulate carbonate sediment; they cannot represent solely rigid crusts, nor can they have been deposited from hydrothermal fluids. The new sedimentological observations independently suggest deposition in a shallow, possibly peritidal carbonate setting, supporting previous interpretations of a sabkha-like environment of deposition (Lowe, 1980, 1983).

3 Construction of Strelley Pool Chert stromatolites from particulate carbonate sediment in a shallow marine, at least occasionally high-energy, setting with robust normal marine geochemical signatures supports a biological interpretation for their origin.

4 Ankerite from ankerite–chert couplets below fossilized microbial mat-like structures in the ~3.49 Ga Dresser Formation also appears to have been precipitated from anoxic seawater on the basis of REE + Y geochemistry.

5 Siderite from banded iron-formation in the Panorama Formation, identified from field and petrographical evidence as hydrothermal in origin, has an REE + Y pattern completely different from the seawater-like patterns found in laminated dolomites. The siderite REE + Y pattern is smooth except for a very strong positive Eu anomaly reminiscent of those found in modern mid-ocean ridge vent waters (e.g. Douville *et al.*, 1999). This discovery supports the widely held conjecture that hydrothermal input into the ocean was more significant during the Archaean than it is today (Derry & Jacobsen, 1990).

6 Siderite in the Panorama Formation was deposited in cyclical variation with jasper. Jasper has REE + Y systematics reminiscent of modified seawater, suggesting that the siderite–jasper association could reflect cyclicity in hydrothermal input into a relatively restricted water body, such as a submerged caldera with limited access to open marine waters. This interpretation is supported by field observations of the Panorama volcanic edifice. Water bodies trapped in calderas could thus have evolved to chemistries and redox states significantly different from the open ocean. Such environments could have harboured life forms that could not survive in the potentially more hostile oceanic environment.

7 The persistence of a positive Eu anomaly in the dolomitic microbial carbonates shows that the 3.45 Ga ocean was anoxic. Eu from hydrothermal vents (such as that sampled by the Panorama siderite) can only be advected and mixed with riverine REE in an anoxic ocean because precipitation of Fe (as oxyhydroxides) from the vent waters in an oxygenated water column leads to complete scavenging of REE and hence to removal of excess Eu.

8 REE geochemistry of the carbonates suggests that terrestrial erosion was already affecting marine REE inventory by ~3.45 Ga, and the absence of a negative Ce anomaly provides additional evidence that both fresh and shallow marine waters were anoxic. Early Archaean seawater appears to have been more depleted in LREE, which could reflect a combination of different pH (Alibert & McCulloch, 1993; Bau & Möller, 1993), redox cycling along an ocean-wide chemocline and preferential removal of LREE in riverine to estuarine environments by scavenging processes during flocculation in an anoxic Archaean shallow hydrosphere.

ACKNOWLEDGEMENTS

We thank the anonymous reviewers and editors, K. O. Konhauser, R. Buick and D. Canfield for their constructive and rapid work, which significantly improved this manuscript. Alan Greig is thanked for expert ICP-MS analyses. B.S.K. is supported by UQ ECR grant 122 4119 52. G.E.W. thanks M. Walter and the Australian Centre for Astrobiology for field support. This paper is published with permission of the Director, Geological Survey of Western Australia.

REFERENCES

Alibert C, McCulloch MT (1993) Rare earth element and neodymium isotopic compositions of the banded iron-formations and associated shales from Hamersley, Western Australia. *Geochimica et Cosmochimica Acta* **57**, 187–204.

Awramik SM, Schopf JW, Walter MR (1983) Filamentous fossil bacteria from the Archean of Western Australia. *Precambrian Research* **20**, 357–374.

Awramik SM, Schopf JW, Walter MR (1988) Carbonaceous filaments from North Pole, Western Australia: are they fossil bacteria in Archean stromatolites? A discussion. *Precambrian Research* **39**, 303–309.

Banner JL, *et al.* (1988) Rare earth element and Nd isotopic variations in regionally extensive dolomites from the Burlington–Keokuk Formation (Mississippian): implications for REE mobility during carbonate diagenesis. *Journal of Sedimentary Petrology* **58**, 415–432.

Barnes KR (1983) *The geology of part of the Strelley Pool Chert, Pilgangoora Syncline, Pilbara Block, Western Australia*. BSc Honours Thesis, University of Western Australia.

Bau M (1999) Scavenging of dissolved yttrium and rare earths by precipitating iron oxyhydroxide: experimental evidence for Ce oxidation, Y–Ho fractionation, and lanthanide tetrad effect. *Geochimica et Cosmochimica Acta* **63**, 67–77.

Bau M, Dulski P (1996) Distribution of yttrium and rare-earth elements in the Penge and Kuruman iron-formations, Transvaal Supergroup, South Africa. *Precambrian Research* **79**, 37–55.

Bau M, Dulski P (1999) Comparing yttrium and rare earths in hydrothermal fluids from the Mid-Atlantic Ridge: implications for Y and REE behaviour during near-vent mixing and for the Y/Ho ratio of Proterozoic seawater. *Chemical Geology* **155**, 77–90.

Bau M, Möller P (1993) Rare earth element systematics of the chemically precipitated component in Early Precambrian iron formations and the evolution of the terrestrial atmosphere-hydrosphere-lithosphere system. *Geochimica et Cosmochimica Acta* **57**, 2239–2249.

Bertand-Sarfati J, Moussine-Pouchkine A (1998) Mauritanian microbial build-ups: Meso-Neoproterozoic stromatolites and

their environment, Field Trip Guidebook. *Publication Des Association Sedimentologistes Francais* **31**.
Bertram CJ, Elderfield H (1993) The geochemical balance of the rare earth elements and neodymium isotopes in the oceans. *Geochimica et Cosmochimica Acta* **57**, 1957–1986.
Brasier MD, Green OR, Jephcoat AP, Kleppe AK, Van Kranendonk MJ, Lindsay JF, Steele A, Grassineau N (2002) Questioning the evidence for Earth's oldest fossils. *Nature* **416**, 76–81.
Buick R (1984) Carbonaceous filaments from North Pole, Western Australia: are they fossil bacteria in Archean stromatolites? *Precambrian Research* **24**, 157–172.
Buick R (1988) Carbonaceous filaments from North Pole, Western Australia: are they fossil bacteria in Archean stromatolites? a reply. *Precambrian Research* **39**, 311–317.
Buick R (1990) Microfossil recognition in Archean rocks: an appraisal of spheroids and filaments from a 3500 M.Y. old chert–barite unit at North Pole, Western Australia. *Palaios* **5**, 441–459.
Buick R, Dunlop JSR (1990) Evaporitic sediments of Early Archaean age from the Warrawoona Group, North Pole, Western Australia. *Sedimentology* **37**, 247–277.
Buick R, Dunlop JSR, Groves DI (1981) Stromatolite recognition in ancient rocks: an appraisal of irregular laminated structures in an early Archaean chert–barite unit from North Pole, Western Australia. *Alcheringa* **5**, 161–181.
Buick R, Groves DI, Dunlop JSR (1995) Abiological origin of described stromatolites older than 3.2 Ga: comment and reply. *Geology* **23**, 191.
Condie KC (1993) Chemical composition and evolution of the upper continental crust: contrasting results from surface samples and shales. *Chemical Geology* **104**, 1–37.
De Baar HJW, Schijf J, Byrne RH (1991) Solution chemistry of the rare earth elements in seawater. *European Journal of Solid State Inorganic Chemistry* **28**, 357–373.
Derry LA, Jacobsen SB (1990) The chemical evolution of Precambrian seawater: evidence from REEs in banded iron formations. *Geochimica et Cosmochimica Acta* **54**, 2965–2977.
Douville E, Bienvenu P, Charlou JL, Donval JP, Fouquet Y, Appriou P, Gamo T (1999) Yttrium and rare earth elements in fluids from various deep-sea hydrothermal systems. *Geochimica et Cosmochimica Acta* **63**, 627–643.
Douville E, Charlou JL, Oelkers EH, Bienvenu P, Jove Colon CF, Donval JP, Fouquet Y, Prieur D, Appriou P (2002) The rainbow vent fluids (36°14′N, MAR): the influence of ultramafic rocks and phase separation on trace metal content in Mid-Atlantic Ridge hydrothermal fluids. *Chemical Geology* **184**, 37–48.
Dunlop JSR, Muir MD, Milne VA, Groves DI (1978) A new microfossil assemblage from the Archaean of Western Australia. *Nature* **274**, 676–678.
Elderfield H (1988) The oceanic chemistry of the rare-earth elements. *Philosophical Transactions of the Royal Society of London* **325**, 105–106.
Fedo CM, Whitehouse MJ (2002) Metasomatic origin of quartz-pyroxene rock, Akilia, Greenland, and implications for Earth's earliest life. *Science* **296**, 1448–1452.
Folk RL (1962) Spectral subdivision of limestone types. In *Classification of Carbonate Rocks* (ed. Ham, WE). *American Association of Petroleum Geologists Memoir* **1**, 62–84.
Gao S, Wedepohl KH (1995) The negative Eu anomaly in Archaean sedimentary rocks – implications for decomposition, age and importance of their granitic sources. *Earth and Planetary Science Letters* **133**, 81–94.
Gibson EK, Jr, McKay DS, Thomas-Keprta KL, Wentworth SJ, Westall F, Steele A, Romanek CS, Blee MS, Toporski J (2001) Life on Mars: evaluation of the evidence within Martian meteorites ALH84001, Nakhla, and Shergotty. *Precambrian Research* **106**, 15–34.
Greaves MJ, Elderfield H, Sholkovitz ER (1999) Aeolian sources of rare earth elements to the Western Pacific Ocean. *Marine Chemistry* **68**, 31–38.
Grotzinger JP (1994) Trends in Precambrian carbonate sediments and their implication for understanding evolution. In *Early Life on Earth, Nobel Symposium 84* (ed. Bengston, S). Columbia University Press, New York, pp. 245–258.
Grotzinger JP, Knoll AH (1995) Anomalous carbonate precipitates: is the Precambrian the key to the Permian? *Palaios* **10**, 578–596.
Grotzinger JP, Rothman DH (1996) An abiotic model for stromatolite morphogenesis. *Nature* **383**, 423–425.
Groves DI, Dunlop JSR, Buick R (1981) An early habitat of life. *Scientific American* **245**, 64–73.
Hofmann HJ, Grey K, Hickman AH, Thorpe R (1999) Origin of 3.45 Ga coniform stromatolites in Warrawoona Group, Western Australia. *Geological Society of America Bulletin* **111**, 1256–1262.
Hoyle J, Elderfield H, Gledhill A, Greaves M (1984) The behaviour of the rare earth elements during mixing of river and sea waters. *Geochimica et Cosmochimica Acta* **48**, 143–149.
Kamber BS, Webb GE (2001) The geochemistry of late Archaean microbial carbonate: implications for ocean chemistry and continental erosion history. *Geochimica et Cosmochimica Acta* **65**, 2509–2525.
Kempe S, Kazmierczak J (1990) Chemistry and stromatolites of the sea-linked Satonda Crater Lake, Indonesia: a recent model for the Precambrian Sea? *Chemical Geology* **81**, 299–310.
Kitajima K, Kabashima T, Ueno Y, Terabayashi M, Maruyama S (2001) Archaean seafloor hydrothermal system in the North Pole of the Pilbara Craton, Western Australia. In: *4th International Archaean Symposium, Extended Abstracts* (eds Cassidy KF, Dunphy JM, Van Kranendonk MJ). *AGSO – Geoscience Australia Record* 2001/37, 51–53.
Konhauser KO, Hamade T, Raiswell R, Morris RC, Ferris FG, Southam G, Canfield DE (2002) Could bacteria have formed the Precambrian banded iron formations? *Geology* **30**, 1079–1082.
Land LS (1992) The quantum theory of dolomite stabilization: does dolomite stabilize by 'Ostwald steps'? In: *Dolomite – from Process and Models to Porosity and Reservoirs 1992 National Conference of Earth Science, Banff, Alberta*. Canadian Society of Petroleum Geologists and Faculty of Extension of the University of Alberta.
Lindsay JF, Brasier MD, McLoughlin N, Green OR, Fogel M, McNamara K, Steele A, Mertzman SA (2003) Abiotic Earth – establishing a baseline for earliest life, data from the Archaean of Western Australia. In: *Lunar and Planetary Institute, Annual Meeting*, Lunar, Planetary Institute Contribution no. 1156, 1137.pdf.
Lipple SL (1975) Definitions of new and revised stratigraphic units of the eastern Pilbara region. *Annual Report – Western Australia, Department of Mines* **1974**, 98–103.
Lowe DR (1980) Stromatolites 3,400-Myr old from the Archaean of Western Australia. *Nature* **284**, 441–443.
Lowe DR (1983) Restricted shallow-water sedimentation of early archean stromatolitic and evaporitic strata of the Strelley Pool Chert, Pilbara Block, Western Australia. *Precambrian Research* **19**, 239–283.
Lowe DR (1994) Abiological origin of described stromatolites older than 3.2 Ga. *Geology* **22**, 387–390.
Lowe DR (1995) Abiological origin of described stromatolites older than 3.2 Ga: comment and reply. *Geology* **23**, 191–192.
Machel HG (1997) Recrystallization versus neomorphism, and the concept of 'significant recrystallization' in dolomite research. *Sedimentary Geology* **113**, 161–168.
Manikyamba C, Naqvi SM (1995) Geochemistry of Fe–Mn formations of the Archaean Sandur schist belt, India – mixing of

clastic and chemical processes at a shallow shelf. *Precambrian Research* **72**, 69–95.
McLennan SM (1989) Rare earth elements in sedimentary rocks: influence of provenance and sedimentary processes. In: *Geochemistry and Mineralogy of Rare Earth Elements* (eds Lipin BR, McKay GA). Mineralogical Society of America, Washington, DC, USA, pp. 169–200.
Michard A, Albarède F (1986) The REE content of some hydrothermal fluids. *Chemical Geology* **55**, 51–60.
Mojzsis SJ, Arrhenius G, McKeegan KD, Harrison TM, Nutman AP, Friend CRL (1996) Evidence for life on Earth before 3,800 million years ago. *Nature* **384**, 55–59.
Nelson DR (2000) Compilation of geochronology data, 1999. *Geological Survey of Western Australia Record* **2002/2**.
Nijman W, De Bruin K, Valkering M (1998) Growth fault control of early Archaean cherts, barite mounds, and chert–barite veins, North Pole Dome, Eastern Pilbara, Western Australia. *Precambrian Research* **88**, 25–52.
Nothdurft LD, Webb GE, Kamber BS (in press) Rare earth element geochemistry of Late Devonian reefal carbonates, Canning Basin, Western Australia. Confirmation of a seawater REE proxy in ancient limestones. *Geochimica et Cosmochimica Acta* **67**, in press.
Nozaki Y, Zhang J, Amakawa H (1997) The fractionation between Y and Ho in the marine environment. *Earth and Planetary Science Letters* **148**, 329–340.
Piepgras DJ, Jacobsen SB (1992) The behavior of rare earth elements in seawater: precise determination of variations in the North Pacific water column. *Geochimica et Cosmochimica Acta* **56**, 1851–1862.
Pope MC, Grotzinger JP, Schreiber BC (2000) Evaporitic subtidal stromatolites produced by *in situ* precipitation: textures, facies associations, and temporal significance. *Journal of Sedimentary Research* **70**, 1139–1151.
Reitner J (1993) Modern cryptic microbialite/metazoan facies from Lizard Island (Great Barrier Reef, Australia). *Facies* **29**, 3–39.
Riding R (2000) Microbial carbonates: the geological record of calcified bacterial–algal mats and biofilms. *Sedimentology* **47** (Suppl. 1), 179–214.
Rosing MT (1999) C-13-depleted carbon microparticl18es in >3700-Ma sea-floor sedimentary rocks from west Greenland. *Science* **283**, 674–676.
Schopf JW (1993) Microfossils of the Early Archaean Apex Chert: new evidence of the antiquity of life. *Science* **260**, 640–646.
Schopf JW, Kudryavtsev AB, Agresti DG, Wdowiak TJ, Czaja AD (2002) Laser-Raman imagery of Earth's earliest fossils. *Nature* **416**, 73–76.
Schopf JW, Packer BM (1987) Early Archaean (3.3 Billion to 3.5 Billion-year-old) microfossils from Warrawoona Group, Australia. *Science* **237**, 70–73.
Schopf JW, Walter MR (1983) Archean microfossils: new evidence of ancient microbes. In: *Earth's Earliest Biosphere* (ed. Schopf JW). Princeton University Press, Princeton, pp. 214–239.
Sholkovitz ER (1992) Chemical evolution of rare earth elements: fractionation between colloidal and solution phases of filtered river water. *Earth and Planetary Science Letters* **114**, 77–84.
Sholkovitz E, Szymczak R (2000) The estuarine chemistry of rare earth elements: comparison of the Amazon, Fly, Sepik and the Gulf of Papua systems. *Earth and Planetary Science Letters* **179**, 299–309.
Tan FC, Hudson JD (1971) Carbon and oxygen isotope relationships of dolomites and co-existing calcites, Great Estuarine Series (Jurassic), Scotland. *Geochimica et Cosmochimica Acta* **35**, 755–767.
Thorpe RI, Hickman AH, Davis DW, Mortensen JK, Trendall AF (1992) Constraints to models for Archaean lead evolution from precise U–Pb geochronology from the Marble Bar region, Pilbara Craton, Western Australia. In *The Archaean: Terrains, Processes and Metallogeny* (eds Glover JE, Ho S). *Geology Department and University Extension, The University of Western Australia, Publication* **22**, 395–408.
Tsikos H, Moore JM (1997) Petrography and geochemistry of the Paleoproterozoic Hotazel Iron-Formation, Kalahari Manganese Field, South Africa: implications for Precambrian manganese metallogenesis. *Economic Geology* **92**, 87–97.
Van Kranendonk MJ (1999) *North Shaw, W.A. sheet 2755.* Western Australia Geological Survey, Perth, 1 : 100 000 Geological Series.
Van Kranendonk MJ (2000) *Geology of the North Shaw 1 : 100 000 sheet.* Western Australia Geological Survey, Perth, 1 : 100 000 Geological Series Explanatory Notes, 86 pp.
Van Kranendonk MJ (in press) Volcanic degassing, hydrothermal circulation and the flourishing of life on Earth: new evidence from the *c.* 3.46 Ga Warrawoona Group, Pilbara Craton, Western Australia. *Precambrian Research* in press.
Van Kranendonk MJ, Collins WJ, Hickman AH, Pawley MJ (in press) Critical tests of vertical vs horizontal tectonic models for the Archaean East Pilbara Granite–Greenstone Terrane, Pilbara Craton, Western Australia. *Precambrian Research* in press.
Van Kranendonk MJ, Hickman AH (2000) Excursion guide to the geology of the North Shaw 1 : 100 000 sheet. *Western Australia Geological Survey, Report* **2000/5**.
Van Kranendonk MJ, Hickman AH, Smithies RH, Nelson DN, Pike G (2002) Geology and tectonic evolution of the Archaean North Pilbara terrain, Pilbara Craton, Western Australia. *Economic Geology* **97**, 695–732.
Van Kranendonk MJ, Hickman AH, Williams IR, Nijman W (2001) Archaean geology of the East Pilbara Granite–Greenstone Terrane Western Australia – a field guide. *Geological Survey of Western Australia, Record* **2001/9**, 134 pp.
Van Kranendonk MJ, Morant P (1998) Revised Archaean stratigraphy of the NORTH SHAW 1 : 100 000 sheet, Pilbara Craton. *Western Australia Geological Survey, Annual Review* **1997–98**, 55–62.
Van Kranendonk MJ, Pirajno F (in press) Geological setting and geochemistry of metabasalts and alteration zones associated with hydrothermal chert ± barite deposits in the ca. 3.45 Ga Warrawoona Group, Pilbara Craton, Australia. *Geochemistry: Exploration, Environment and Analysis* in press.
Van Zuilen MA, Lepland A, Arrhenius G (2002) Reassessing the evidence for the earliest traces of life. *Nature* **418**, 627–630.
Walter MR, Buick R, Dunlop JSR (1980) Stromatolites, 3400–3500 Myr old from the North Pole area, Western Australia. *Nature* **284**, 443–445.
Webb GE, *et al.* (1998) Inferred syngenetic textural evolution in Holocene cryptic reefal microbialites, Heron Reef, Great Barrier Reef, Australia. *Geology* **26**, 355–358.
Webb GE, Kamber BS (2000) Rare earth elements in Holocene reefal microbialites: a new shallow seawater proxy. *Geochimica et Cosmochimica Acta* **64**, 1557–1565.
Wheat CG, Mottl MJ, Rudnicki M (2002) Trace element and REE composition of a low-temperature ridge-flank hydrothermal spring. *Geochimica et Cosmochimica Acta* **66**, 3693–3705.
Yamashita K, Creaser RA (1999) Geochemical and Nd isotopic constraints for the origin of Late Archean turbidites from the Yellowknife area, Northwest Territories, Canada. *Geochimica et Cosmochimica Acta* **63**, 2579–2598.
Zhong S, Mucci A (1995) Partitioning of rare earth elements (REEs) between calcite and seawater solutions at 25 °C and 1 atm, and high dissolved REE concentrations. *Geochimica et Cosmochimica Acta* **59**, 443–453.